

<sup>1</sup> Transcripts with high distal heritability mediate genetic effects on  
<sup>2</sup> complex metabolic traits

<sup>3</sup>

<sup>4</sup> Anna L. Tyler, J. Matthew Mahoney, Mark P. Keller, Candice N. Baker, Margaret Gaca, Anuj Srivastava,  
<sup>5</sup> Isabela Gerdes Gyuricza, Madeleine J. Braun, Nadia A. Rosenthal, Alan D. Attie, Gary A. Churchill and  
<sup>6</sup> Gregory W. Carter

<sup>7</sup> **Abstract**

<sup>8</sup> Although many genes are subject to local regulation, recent evidence suggests that complex distal regulation  
<sup>9</sup> may be more important in mediating phenotypic variability. To assess the role of distal gene regulation in  
<sup>10</sup> complex traits, we combined multi-tissue transcriptomes with physiological outcomes to model diet-induced  
<sup>11</sup> obesity and metabolic disease in a population of Diversity Outbred mice. Using a novel high-dimensional  
<sup>12</sup> mediation analysis, we identified a composite transcriptome signature that summarized genetic effects on  
<sup>13</sup> gene expression and explained 30% of the variation across all metabolic traits. The signature was heritable,  
<sup>14</sup> interpretable in biological terms, and predicted obesity status from gene expression in an independently  
<sup>15</sup> derived mouse cohort and multiple human studies. Transcripts contributing most strongly to this composite  
<sup>16</sup> mediator frequently had complex, distal regulation distributed throughout the genome. These results suggest  
<sup>17</sup> that trait-relevant variation in transcription is largely distally regulated, but is nonetheless identifiable,  
<sup>18</sup> interpretable, and translatable across species.

<sup>19</sup> **Introduction**

<sup>20</sup> Evidence from genome-wide association studies (GWAS) suggests that most heritable variation in complex  
<sup>21</sup> traits is mediated through regulation of gene expression. The majority of trait-associated variants lie  
<sup>22</sup> in gene regulatory regions<sup>1–7</sup>, suggesting a relatively simple causal model in which a variant alters the  
<sup>23</sup> homeostatic expression level of a nearby (local) gene which, in turn, alters a trait. Statistical methods such  
<sup>24</sup> as transcriptome-wide association studies (TWAS)<sup>8–11</sup> and summary data-based Mendelian randomization  
<sup>25</sup> (SMR)<sup>10</sup> have used this idea to identify genes associated with multiple disease traits<sup>12–15</sup>. However, despite

26 the great promise of these methods, explaining trait effects with local gene regulation has been more difficult  
27 than initially assumed<sup>16;17</sup>. Although trait-associated variants typically lie in non-coding, regulatory regions,  
28 these variants often have no detectable effects on gene expression<sup>16</sup> and tend not to co-localize with expression  
29 quantitative trait loci (eQTLs)<sup>17;18</sup>. These observations suggest that the relationship among genetic variants,  
30 gene expression, and organism-level traits is more complex than the simple, local model.

31 In recent years the conversation around the genetic architecture of common disease traits has been addressing  
32 this complexity, and there is increased interest in more distant (distal) genetic effects as potential drivers  
33 of trait variation<sup>18–20;15;21</sup>. In general, distal effects are defined as being greater than 4 or 5Mb away from  
34 the transcription start site of a given gene. We use the terms local and distal rather than *cis* and *trans*  
35 because *cis* and *trans* have specific biochemical meanings<sup>22</sup>, whereas local and distal are defined only by  
36 genomic position. The importance of distal genetic effects is proposed in the omnigenic model, which posits  
37 that trait-driving genes are cumulatively influenced by many distal variants. In this view, the heritable  
38 transcriptomic signatures driving clinical traits are an emergent state arising from the myriad molecular  
39 interactions defining and constraining gene expression. Consistent with this view, it has been suggested  
40 that part of the difficulty in explaining trait variation through local eQTLs may arise in part because gene  
41 expression is not measured in the appropriate cell types<sup>16</sup>, or cell states<sup>23</sup>, and thus local eQTLs influencing  
42 traits cannot be detected in bulk tissue samples. This context dependence emphasizes the essential role of  
43 complex regulatory and tissue networks in mediating variant effects. The mechanistic dissection of complex  
44 traits in this model is more challenging because it requires addressing network-mediated effects that are  
45 weaker and greater in number. However, the comparative importance of distal effects over local effects is  
46 currently only conjectured and extremely challenging to address in human populations.

47 To assess the role of wide-spread distal gene regulation in the genetic architecture of complex traits, we used  
48 genetically diverse mice as a model system. In mice we can obtain simultaneous measurements of the genome,  
49 transcriptome, and phenome in all individuals. We used diet-induced obesity and metabolic disease as an  
50 archetypal example of a complex trait. In humans, these phenotypes are genetically complex with hundreds of  
51 variants mapped through GWAS<sup>24;25</sup> that are known to act through multiple tissues<sup>26;27</sup>. Likewise in mice,  
52 metabolic traits are also genetically complex<sup>28</sup> and synteny analysis implicates a high degree of concordance  
53 in the genetic architecture between species<sup>28;12</sup>. Furthermore, in contrast to humans, in mice we have access  
54 to multiple disease-relevant tissues in the same individuals with sufficient numbers for adequate statistical  
55 power.

56 We generated two complementary data sets: a discovery data set in a large population of Diversity Outbred  
57 (DO) mice<sup>29</sup>, and an independent validation data set derived by crossing inbred strains from the Collaborative

58 Cross (CC) recombinant inbred lines<sup>30</sup> to form CC recombinant inbred intercross (CC-RIX) mice. Both  
59 populations were maintained on a high-fat, high-sugar diet to model diet-induced obesity and metabolic  
60 disease<sup>12</sup>.

61 The DO population and CC recombinant inbred lines were derived from the same eight inbred founder  
62 strains: five classical lab strains and three strains more recently derived from wild mice<sup>29</sup>, representing three  
63 subspecies and capturing 90% of the known variation in laboratory mice<sup>31</sup>. The DO mice are maintained  
64 with a breeding scheme that ensures equal contributions from each founder across the genome thus rendering  
65 almost the whole genome visible to genetic inquiry and maximizing power to detect eQTLs<sup>29</sup>. The CC mice  
66 were initially intercrossed to recombine the genomes from all eight founders, and then inbred for at least 20  
67 generations to create recombinant inbred lines<sup>30;32;31</sup>. Because these two populations have common ancestral  
68 haplotypes but highly distinct kinship structure, we could directly and unambiguously compare the local  
69 genetic effects on gene expression at the whole-transcriptome level while varying the population structure  
70 driving distal regulation.

71 In the DO population, we paired clinically relevant metabolic traits, including body weight and plasma levels  
72 of insulin, glucose and lipids<sup>12</sup>, with transcriptome-wide gene expression in four tissues related to metabolic  
73 disease: adipose tissue, pancreatic islets, liver, and skeletal muscle. We measured similar metabolic traits  
74 in a CC-RIX population and gene expression from three of the four tissues used in the DO: adipose tissue,  
75 liver, and skeletal muscle. Measuring gene expression in multiple tissues is critical to adequately assess the  
76 extent to which local gene regulation varies across the tissues and whether such variability might account for  
77 previous failed attempts to identify trait-relevant local eQTLs. The CC-RIX carry the same founder alleles  
78 as the DO. Thus, local gene regulation is expected to match between the populations. However, because  
79 the alleles are recombined throughout the genome, distal effects are expected to vary from those in the DO,  
80 allowing us to directly assess the role of distal gene regulation in driving trait-associated transcript variation.  
81 To mechanistically dissect distal effects on metabolic disease, we developed a novel dimension reduction  
82 framework called high-dimensional mediation analysis (HDMA) to identify the heritable transcriptomic  
83 signatures driving trait variation, which we compared between mouse populations and to human data sets  
84 with measured adipose gene expression. Together, these data enable a comprehensive view into the genetic  
85 architecture of metabolic disease.

86 **Results**

87 **Genetic variation contributed to wide phenotypic variation**

88 Although the environment was consistent across the DO mice, the genetic diversity present in this population  
89 resulted in widely varying distributions across physiological measurements (Fig. 1). For example, body  
90 weights of adult individuals varied from less than the average adult C57BL/6J (B6) body weight to several  
91 times the body weight of a B6 adult in both sexes (Males: 18.5 - 69.1g, Females: 16.0 - 54.8g) (Fig. 1A).  
92 Fasting blood glucose (FBG) also varied considerably (Fig. 1B), although few of the animals had FBG levels  
93 that would indicate pre-diabetes (19 animals, 3.8%), or diabetes (7 animals, 1.4%) according to previously  
94 developed cutoffs (pre-diabetes:  $\text{FBG} \geq 250 \text{ mg/dL}$ , diabetes:  $\text{FBG} \geq 300 \text{ mg/dL}$ )<sup>33</sup>. Males had higher  
95 FBG than females on average (Fig. 1C) as has been observed before suggesting either that males were more  
96 susceptible to metabolic disease on the high-fat, high-sugar (HFHS) diet, or that males and females may  
97 require different thresholds for pre-diabetes and diabetes.

98 Body weight was strongly positively correlated with food consumption (Fig. 1D  $R^2 = 0.51, p < 2.2 \times 10^{-16}$ )  
99 and FBG (Fig. 1E,  $R^2 = 0.21, p < 2.2 \times 10^{-16}$ ) suggesting a link between behavioral factors and metabolic  
100 disease. However, the heritability of this trait and others (Fig. 1F) indicates that genetics contribute  
101 substantially to correlates of metabolic disease in this population.

102 The trait correlations (Fig. 1G) showed that most of the metabolic trait pairs were only modestly correlated,  
103 which, in conjunction with the trait decomposition (Supp. Fig. S1), suggests complex relationships among  
104 the measured traits and a broad sampling of multiple heritable aspects of metabolic disease including overall  
105 body weight, glucose homeostasis, and pancreatic function.

106 **Distal Heritability Correlated with Phenotype Relevance**

107 It is widely assumed that variation in traits is mediated through local regulation of gene expression. To test  
108 this assumption, we measured transcriptome-wide gene expression in four tissues—adipose, liver, pancreatic  
109 islet, and skeletal muscle—in the DO cohort. (Basic results from a standard eQTL analysis<sup>34</sup> (Methods)  
110 are available in Supp. Fig. S2). We estimated the local genetic contribution to each transcript as the  
111 variance explained by the haplotype probabilities at the genetic marker closest to the gene transcription  
112 start site. We estimated the distal heritability as the heritability of the residuals after local haplotype had  
113 been accounted for (Methods). Importantly, this estimate was not based on distal eQTL, but rather the  
114 unlocalized contribution of the genome after removing the local genetic effect.

115 Overall, local and distal genetic factors contributed approximately equally to transcript abundance. In all

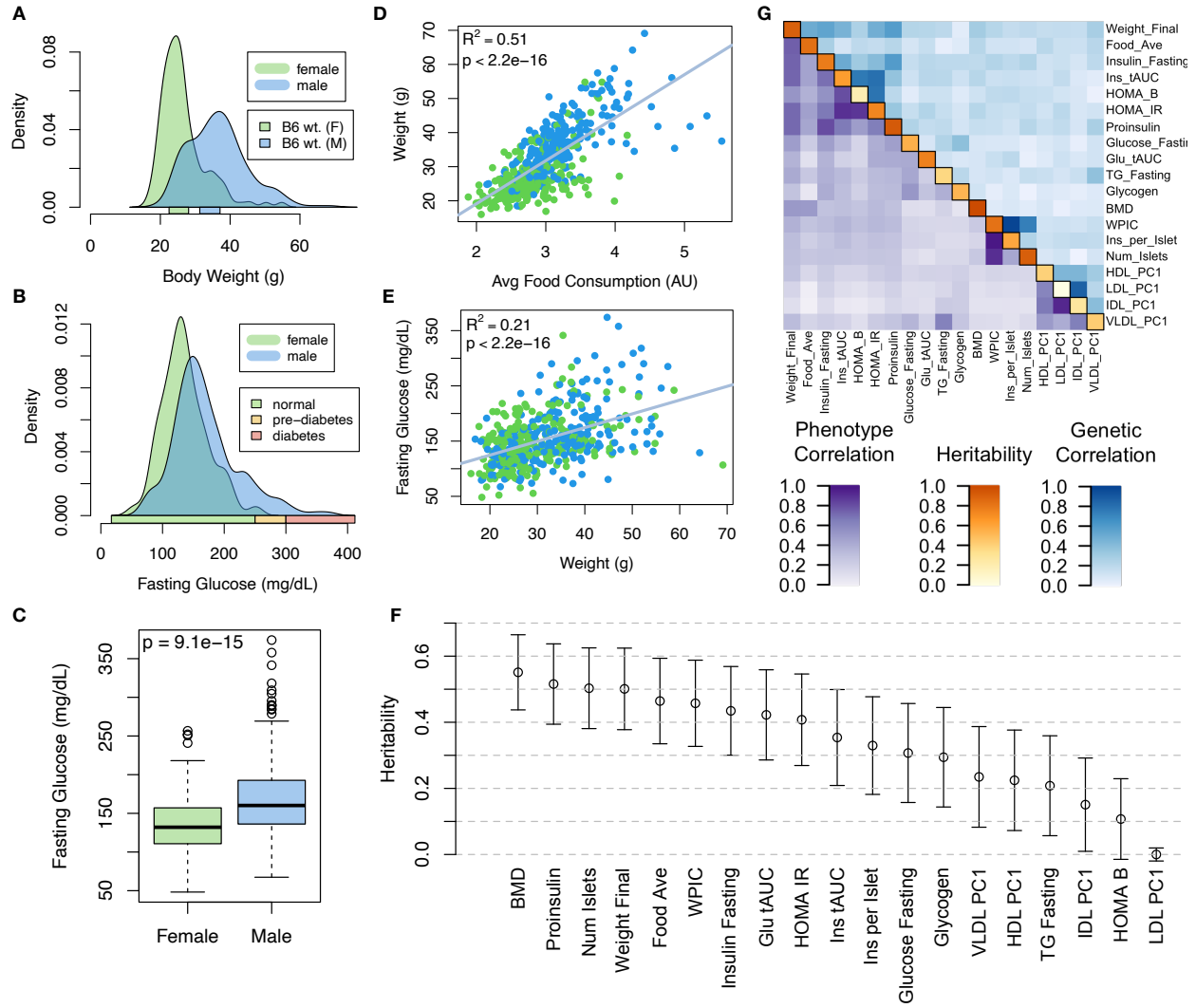


Figure 1: Clinical overview. **A.** Distributions of final body weight in the diversity outbred mice. Sex is indicated by color. The average B6 male and female adult weights at 24 weeks of age are indicated by blue and green bars on the x-axis. **B.** The distribution of final fasting glucose across the population split by sex. Normal, pre-diabetic, and diabetic fasting glucose levels for mice are shown by colored bars along the x-axis. **C.** Males had higher fasting blood glucose on average than females ( $p = 9.1 \times 10^{-15}$ ). **D.** The relationship between food consumption and body weight for both sexes. **E.** Relationship between body weight and fasting glucose for both sexes. **F.** Heritability estimates for each physiological trait. Bars show standard error of the estimate. **G.** Correlation structure between pairs of physiological traits. The lower triangle shows Pearson correlation coefficients between pairs of traits ( $r$ ). The upper triangle shows the Pearson correlation coefficient ( $r$ ) between LOD traces of pairs of traits, and diagonal shows the estimated heritability of each trait. BMD - bone mineral density, WPIC - whole pancreas insulin content, Glu tAUC - glucose total area under the curve, HOMA IR - homeostatic measurement of insulin resistance, HOMA B - homeostatic measure of beta cell health, VLDL - very low-density lipoprotein, LDL - low-density lipoprotein, IDL - intermediate density lipoprotein, HDL - high-density lipoprotein, TG - triglyceride.

tissues, both local and distal factors explained between 8 and 17% of the variance in the median transcript (Fig, 2A).

118 The 50% contribution of local genetic variation to transcript abundance contrasts with findings in humans in  
119 which local variants have been found to explain only 20-30% of total heritability, while distal effects explain  
120 the remaining 70-80%<sup>35;36</sup>. This discrepancy may arise due to the high degree of linkage disequilibrium in the  
121 DO mice compared to human populations and to the high degree of confidence with which we can estimate  
122 ancestral haplotypes in this population. At each position in the mice we can estimate ancestral haplotype  
123 with a high degree of accuracy. Haplotype at any given genetic marker captures genomic information from  
124 a relatively large genomic region surrounding each marker. In contrast, there is a much higher degree of  
125 recombination in human populations and ancestral haplotypes are more numerous and more difficult to  
126 estimate than in the mice. Thus in the mice, each marker may capture more local regulatory variation than  
127 SNPs or estimated haplotypes capture in humans. It has been found that transcripts with multiple local eQTL  
128 have higher local heritability than transcripts with single local eQTL<sup>37</sup>. Because of the high diversity in the  
129 DO and the high rates of linkage disequilibrium, it is possible that there are more local variants regulating  
130 transcription creating a proportionally larger effect of local regulation.

131 To assess the importance of genetic regulation of transcript levels to clinical traits, we compared the local  
132 and distal heritabilities of transcripts to their trait relevance. We defined trait relevance for a transcript as  
133 its maximum absolute Spearman correlation coefficient ( $\rho$ ) across all traits (Methods). The local heritability  
134 of transcripts was negatively associated with their trait relevance (Fig. 2B), suggesting that the more  
135 local genotype influenced transcript abundance, the less effect this variation had on the measured traits.  
136 Conversely, the distal heritability of transcripts was positively associated with trait relevance (Fig. 2C). That  
137 is, transcripts that were more highly correlated with the measured traits tended to be distally, rather than  
138 locally, heritable. Importantly, this pattern was consistent across all tissues. This finding is also consistent  
139 with previous observations that transcripts with low local heritability explain more expression-mediated  
140 disease heritability than transcripts with high local heritability<sup>19</sup>. However, the positive relationship between  
141 trait correlation and distal heritability demonstrated further that there are diffuse genetic effects throughout  
142 the genome converging on trait-related transcripts.

143 **High-Dimensional Mediation Analysis identified a high-heritability composite trait that was  
144 mediated by a composite transcript**

145 The above univariate analyses establish the importance of distal heritability for trait-relevant transcripts.  
146 However, the number of transcripts dramatically exceeds the number of phenotypes. Thus, we expect the  
147 heritable, trait-relevant transcripts to be highly correlated and organized according to coherent, biological  
148 processes representing the mediating endophenotypes driving clinical trait variation. To identify these

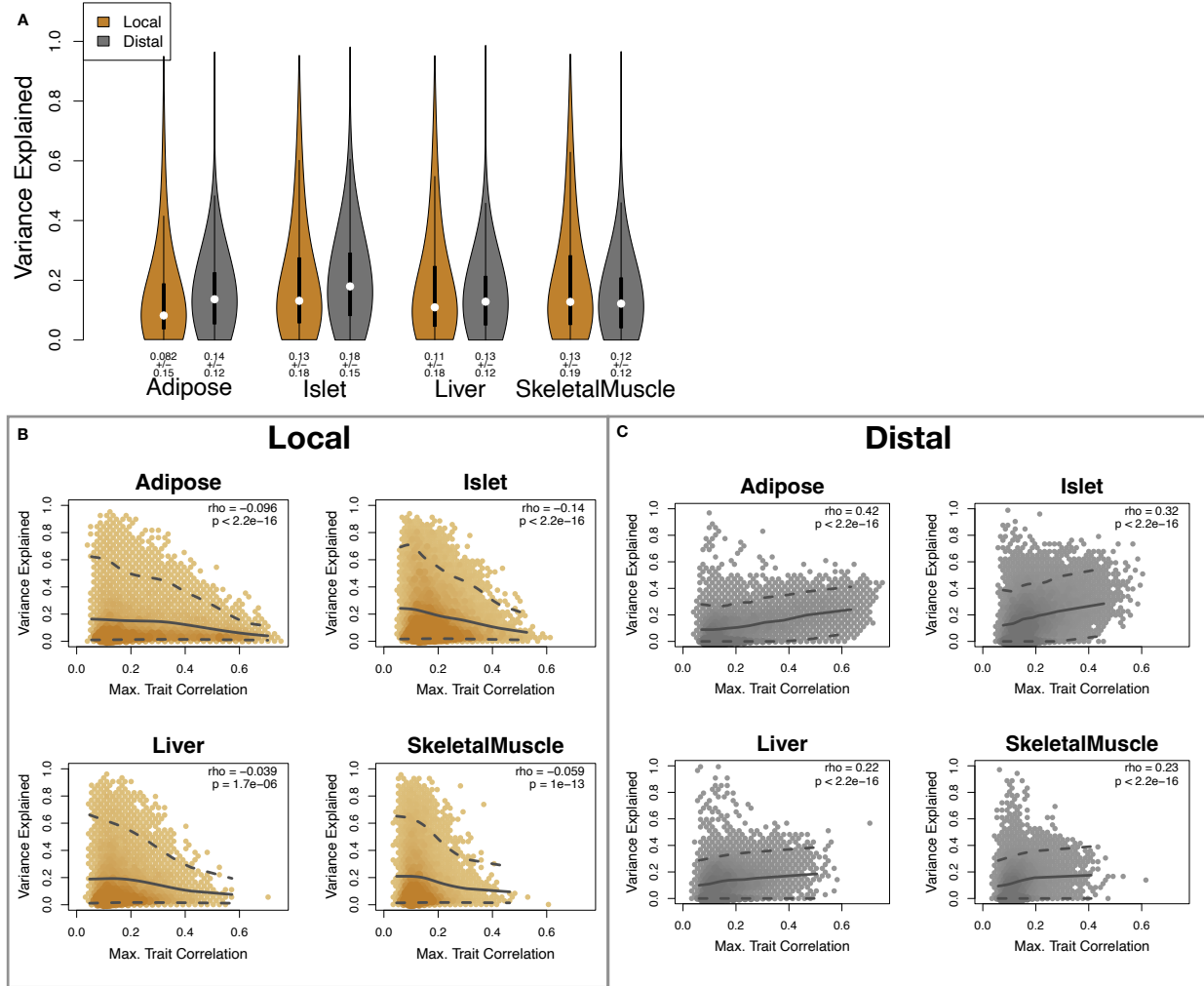


Figure 2: Transcript heritability and trait relevance. **A.** Distributions of local and distal heritability of transcripts across the four tissues. Overall local and distal factors contributed equally to transcript heritability. The relationship between **(B.)** local and **(C.)** distal heritability and trait relevance across all four tissues. Here trait relevance is defined as the maximum correlation between the transcript and all traits. The upper and lower dashed line in each panel show the 95th and 5th percentile correlation. The solid line shows the mean trait correlation in transcripts with increasing variance explained either locally (B) or distally (C). Transcripts that are highly correlated with traits tended to have low local heritability and high distal heritability.

149 endophenotypes in a theoretically principled way, we developed a novel dimension-reduction technique,  
 150 high-dimension mediation analysis (HDMA), that uses the theory of causal graphical models to identify a  
 151 transcriptomic signature that is simultaneously 1) highly heritable, 2) strongly correlated to the measured  
 152 phenotypes, and 3) conforms to the causal mediation hypothesis (Fig. 3). In HDMA, we first use a  
 153 linear mapping called kernelization to dimension-reduce the genome, transcriptome, and phenotype to kernel  
 154 matrices  $G_K$ ,  $T_K$  and  $P_K$  respectively, which each have the dimensions  $n$  by  $n$  where  $n$  is the number  
 155 of individuals (Methods). These kernel matrices describe the relationships among the individual mice in  
 156 genome space, transcriptome space, and phenotype space and ensure that these three omic spaces have

157 the same dimensions, and thus the same weight in the analysis. If not dimension-reduced, the transcriptome  
158 would outweigh the genome in the model. We then projected these  $n \times n$ -dimensional kernel matrices  
159 onto one-dimensional scores—a composite genome score ( $G_C$ ), a composite transcriptome score ( $T_C$ ), and a  
160 composite phenome score ( $P_C$ )—and used the univariate theory of mediation to constrain these projections to  
161 satisfy the hypotheses of perfect mediation, namely that upon controlling for the transcriptomic score, the  
162 genome score is uncorrelated to the phenome score. A complete mathematical derivation and implementation  
163 details for HDMA are available in the Methods.

164 Using HDMA we identified the major axis of variation in the transcriptome that was consistent with mediating  
165 the effects of the genome on metabolic traits (Fig 3). Fig. 3A shows the partial correlations ( $\rho$ ) between  
166 the pairs of these composite vectors. The partial correlation between  $G_C$  and  $T_C$  was 0.42, and the partial  
167 correlation between  $T_C$  and  $P_C$  was 0.78. However, when the transcriptome was taken into account, the  
168 partial correlation between  $G_C$  and  $P_C$  was effectively zero (0.039).  $P_C$  captured 30% of the overall trait  
169 variance, and its estimated heritability was  $0.71 \pm 0.084$ , which was higher than any of the measured traits  
170 (Fig. 1F). Thus, HDMA identified a maximally heritable metabolic composite trait and a highly heritable  
171 component of the transcriptome that are correlated as expected in the perfect mediation model.

172 As discussed in the Methods, HDMA is related to a generalized form of canonical correlation analysis (CCA).  
173 Standard CCA is prone to over-fitting because in any two large matrices it can be trivial to identify highly  
174 correlated composite vectors<sup>38</sup>. To assess whether our implementation of HDMA was similarly prone to  
175 over-fitting in a high-dimensional space, we performed permutation testing. We permuted the individual  
176 labels on the transcriptome matrix 10,000 times and recalculated the path coefficient, which is the correlation  
177 of  $G_C$  and  $T_C$  multiplied by the correlation of  $T_C$  and  $P_C$ . This represents the strength of the path from  
178  $G_C$  to  $P_C$  that is putatively mediated through  $T_C$ . The permutations preserved the correlation between the  
179 genome and phenome, but broke the correlations between the genome and the transcriptome, as well as  
180 between the transcriptome and the phenome. We could thus test whether, given a random transcriptome,  
181 HDMA would overfit and identify apparently mediating transcriptomic signatures in random data. The null  
182 distribution of the path coefficient is shown in Fig. 3B, and the observed path coefficient from the original  
183 data is indicated by a red line. The observed path coefficient was well outside the null distribution generated  
184 by permutations ( $p < 10^{-16}$ ). Fig. 3C illustrates this observation in more detail. Although we identified  
185 high correlations between  $G_C$  and  $T_C$ , and modest correlations between  $T_C$  and  $P_C$  in the null data (Fig 3C),  
186 these two values could not be maximized simultaneously in the null data. In contrast, the red dot shows that  
187 in the real data both the  $G_C$ - $T_C$  correlation and the  $T_C$ - $P_C$  correlation could be maximized simultaneously  
188 suggesting that the path from genotype to phenotype through the transcriptome is highly non-trivial and

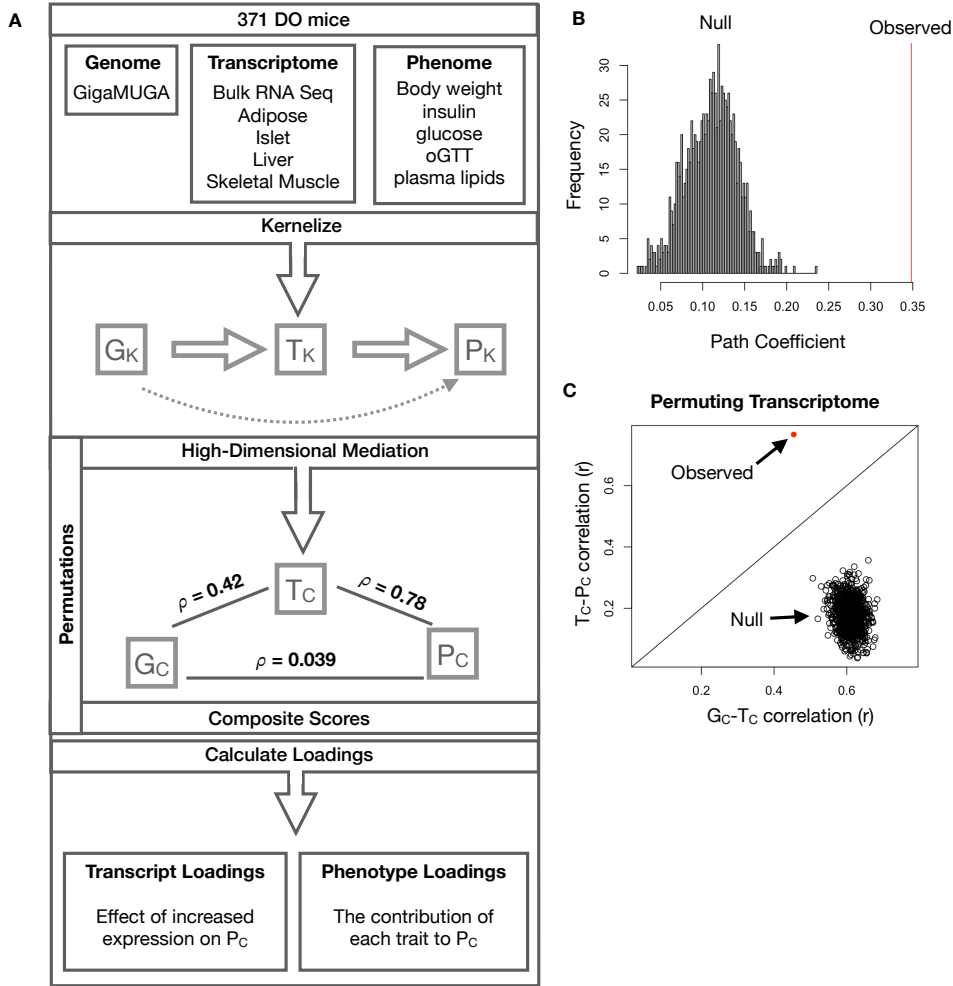


**Figure 3: High-dimensional mediation.** **A.** Workflow indicating major steps of high-dimensional mediation. The genotype, transcriptome, and phenotype matrices were independently normalized and converted to kernel matrices representing the pairwise relationships between individuals for each data modality ( $G_K$  = genome kernel,  $T_K$  = transcriptome kernel;  $P_K$  = phenome kernel). High-dimensional mediation was applied to these matrices to maximize the direct path  $G \rightarrow T \rightarrow P$ , the mediating pathway (arrows), while simultaneously minimizing the direct  $G \rightarrow P$  pathway (dotted line). The composite vectors that resulted from high-dimensional mediation were  $G_C$ ,  $T_C$ , and  $P_C$ . The partial correlations  $\rho$  between these vectors indicated perfect mediation. Transcript and trait loadings were calculated as described in the Methods. **B.** The null distribution of the path coefficient derived from 10,000 permutations compared to the observed path coefficient (red line). **C.** The null distribution of the  $G_C$ - $T_C$  correlation vs. the  $T_C$ - $P_C$  correlation compared with the observed value (red dot).

189 identifiable in this case. These results suggest that these composite vectors represent genetically determined  
190 variation in phenotype that is mediated through genetically determined variation in transcription.

191 **Body weight and insulin resistance were highly represented in the expression-mediated com-**  
192 **posite trait**

193 Each composite score is a weighted combination of the measured variables. The magnitude and sign of  
194 the weights, called loadings, correspond to the relative importance and directionality of each variable in  
195 the composite score. The loadings of each measured trait onto  $P_C$  indicate how much each contributed  
196 to the composite phenotype. Body weight contributed the most (Fig. 4), followed by homeostatic insulin  
197 resistance (HOMA\_IR) and fasting plasma insulin levels (Insulin\_Fasting). We can thus interpret  $P_C$  as an  
198 index of metabolic disease (Fig. 4B). Individuals with high values of  $P_C$  have a higher metabolic disease  
199 index (MDI) and greater metabolic disease, including higher body weight and higher insulin resistance. We  
200 refer to  $P_C$  as MDI going forward. Traits contributing the least to MDI were measures of cholesterol and  
201 pancreas composition. Thus, when we interpret the transcriptomic signature identified by HDMA, we are  
202 explaining primarily the putative transcriptional mediation of body weight and insulin resistance, as opposed  
203 to cholesterol measurements.

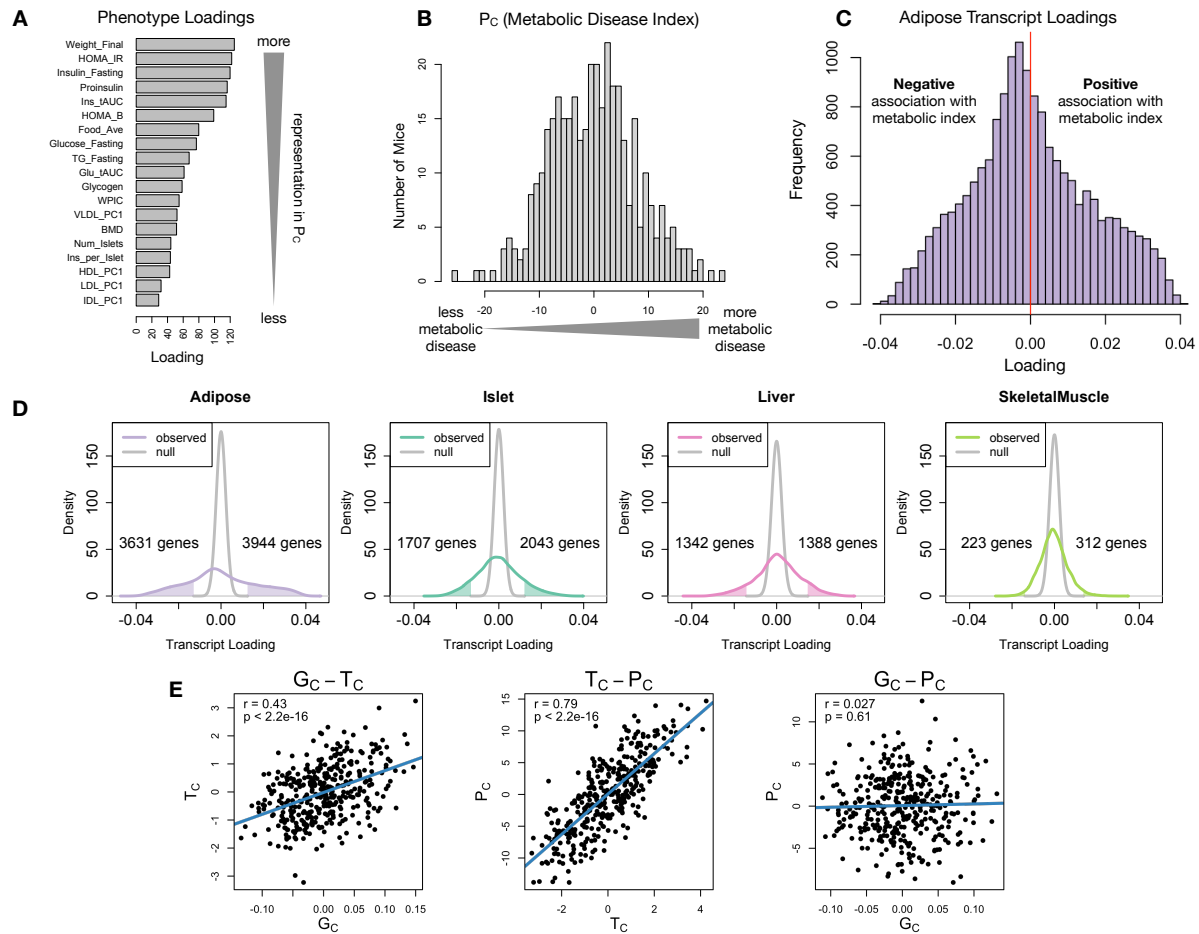


Figure 4: Interpretation of loadings. **A.** Loadings across traits. Body weight and insulin resistance contributed the most to the composite trait. **B.** Phenotype scores across individuals. Individuals with large positive phenotype scores had higher body weight and insulin resistance than average. Individuals with large negative phenotype scores had lower body weight and insulin resistance than average. **C.** Distribution of transcript loadings in adipose tissue. For transcripts with large positive loadings, higher expression was associated with higher phenotype scores. For transcripts with large negative loadings, higher expression was associated with lower phenotype scores. **D.** Distributions of loadings across tissues compared to null distributions. Shaded areas represent loadings that were more extreme than the null distribution. Numbers indicate how many transcripts had loadings above and below the extremes of the null. Transcripts in adipose tissue had the most extreme loadings indicating that transcripts in adipose tissue were the best mediators of the genetic effects on body weight and insulin resistance. **E.** Scatter plots showing correlations between composite vectors for the genome ( $G_C$ ), the transcriptome ( $T_C$ ), and the phenome ( $P_C$ ). The  $G_C - T_C$  correlation is high, the  $T_C - P_C$  correlation is high, and there is no significant correlation between  $G_C$  and  $P_C$ . This correlation structure is consistent with perfect mediation.

- 204 **High-loading transcripts had low local heritability, high distal heritability, and were linked  
205 mechanistically to obesity**
- 206 We interpreted large loadings onto transcripts as indicating strong mediation of the effect of genetics on  
207 MDI. Large positive loadings indicate that higher expression was associated with a higher MDI (i.e. higher

208 risk of obesity and metabolic disease on the HFHS diet) (Fig. 4C-D). Conversely, large negative loadings  
209 indicate that high expression of these transcripts was associated with a lower MDI (i.e. lower risk of obesity  
210 and metabolic disease on the HFHS diet) (Fig. 4C-D). Fig. 4D compares the observed transcript loading  
211 distributions to null distributions and indicates how many transcripts in each tissue had large positive and  
212 negative loadings. A direct comparison of the tissues can be seen in Supp. Fig. S3. We used gene set  
213 enrichment analysis (GSEA)<sup>39;40</sup> to look for biological processes and pathways that were enriched at the top  
214 and bottom of this list (Methods).

215 In adipose tissue, both GO processes and KEGG pathway enrichments pointed to an axis of inflammation  
216 and metabolism (Figs. S4 and S5). GO terms and KEGG pathways associated with inflammation were  
217 positively associated with MDI, indicating that increased expression in inflammatory pathways was associated  
218 with a higher burden of disease. It is well established that adipose tissue in obese individuals is inflamed  
219 and infiltrated by macrophages<sup>41–45</sup>, and the results here suggest that this may be a dominant heritable  
220 component of metabolic disease.

221 The strongest negative enrichments in adipose tissue were related to mitochondrial activity in general, and  
222 thermogenesis in particular (Figs. S4 and S5). Genes in the KEGG oxidative phosphorylation pathway were  
223 almost universally negatively loaded in adipose tissue, suggesting that increased expression of these genes was  
224 associated with reduced MDI (Supp. Fig. S6). Consistent with this observation, it has been shown previously  
225 that mouse strains with greater thermogenic potential are also less susceptible to obesity on an obesigenic  
226 diet<sup>46</sup>.

227 Transcripts associated with the citric acid cycle as well as the catabolism of the branched-chain amino acids  
228 (valine, leucine, and isoleucine) were strongly enriched with negative loadings in adipose tissue (Supp. Figs.  
229 S4, S7 and S8). Expression of genes in both pathways (for which there is some overlap) has been previously  
230 associated with insulin sensitivity<sup>12;47;48</sup>, suggesting that heritable variation in regulation of these pathways  
231 may influence risk of insulin resistance.

232 Looking at the 10 most positively and negatively loaded transcripts from each tissue, it is apparent that  
233 transcripts in the adipose tissue had the largest loadings, both positive and negative (Fig. 5A bar plot). This  
234 suggests that much of the effect of genetics on body weight and insulin resistance is mediated through gene  
235 expression in adipose tissue. This finding does not speak to the relative importance of tissues not included  
236 in this study, such as brain, in which transcriptional variation may mediate a large portion of the genetic  
237 effect on obesity. The strongest loadings in liver and pancreas were comparable, and those in skeletal muscle  
238 were the weakest (Fig. 5A), suggesting that less of the genetic effects were mediated through transcription

239 in skeletal muscle. As expected, heritability analysis showed that transcripts with the largest loadings had  
240 higher distal heritability than local heritability (Fig. 5A heat map and box plot). We also performed TWAS  
241 in this population by imputing transcript levels for each gene based on local genotype only and correlating the  
242 imputed transcript levels with each trait. In contrast to HDMA, the TWAS procedure tended to nominate  
243 transcripts with lower loadings (Fig. 5B), higher local heritability and lower distal heritability. Finally, we  
244 focused on transcripts with the highest local heritability in each tissue (Fig. 5C). This procedure selected  
245 transcripts with low loadings on average, consistent with our findings above (Fig. 2B).

246 We performed a literature search for the genes in each of these groups along with the terms “diabetes”,  
247 “obesity”, and the name of the expressing tissue to determine whether any of these genes had previous  
248 associations with metabolic disease in the literature (Methods). Multiple genes in each group had been  
249 previously associated with obesity and diabetes (Fig. 5 bolded gene names). Genes with high loadings were  
250 most highly enriched for previous literature support. They were 2.2 times more likely than TWAS hits and 4  
251 times more likely than genes with high local heritability to be previously associated with obesity or diabetes.

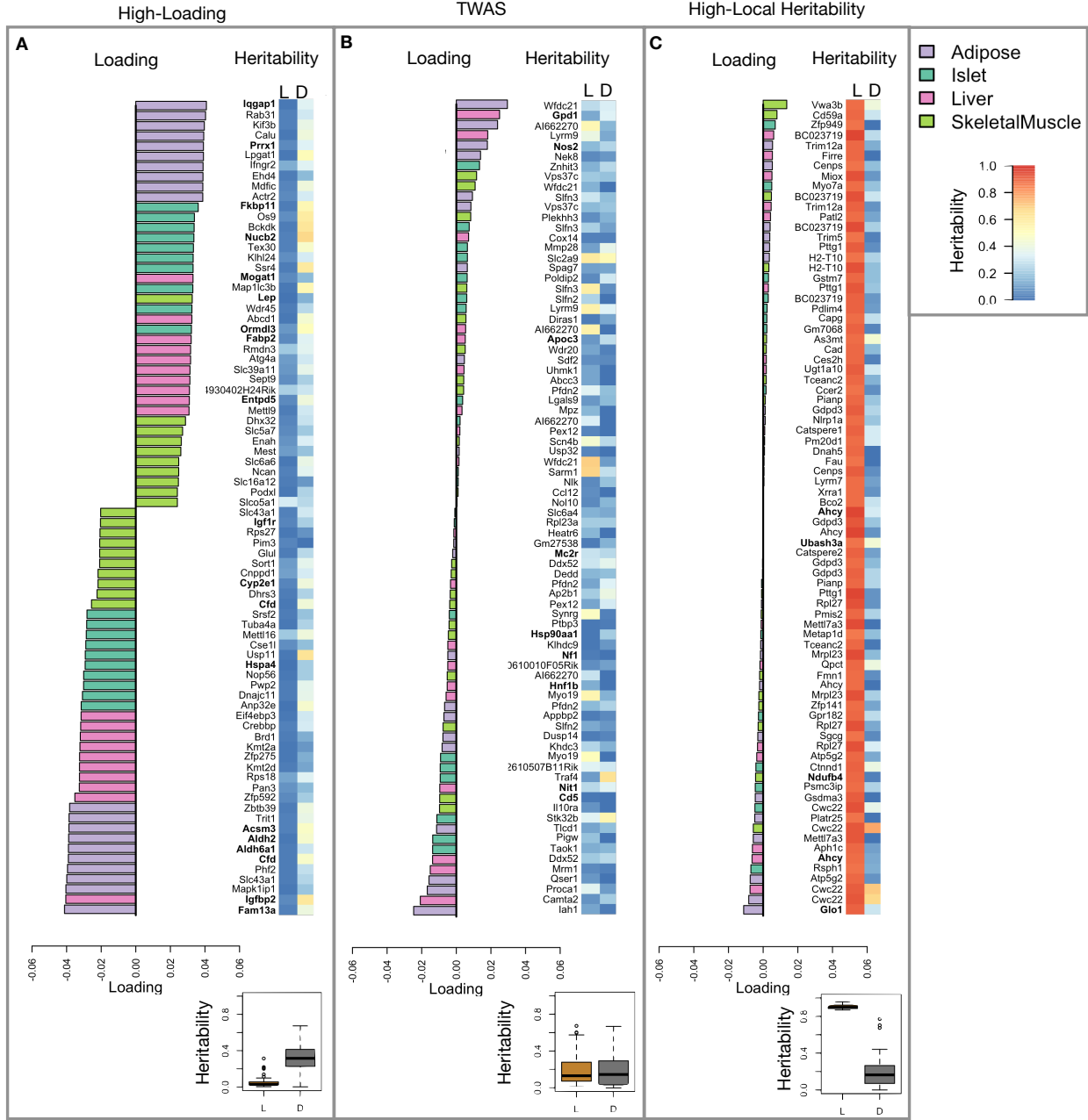


Figure 5: Transcripts with high loadings have high distal heritability and literature support (bolded gene names). Each panel has a bar plot showing the loadings of transcripts selected by different criteria. Bar color indicates the tissue of origin. The heat map shows the local (L - left) and distal (D - right) heritability of each transcript. **A.** Loadings for the 10 transcripts with the largest positive loadings and the 10 transcripts with the largest negative loadings for each tissue. Distal heritability was significantly higher than local heritability (t-test  $p < 2.2^{-16}$ ). **B.** Loadings of TWAS candidates with the 10 largest positive correlations with traits and the largest negative correlations with traits across all four tissues. Local and distal heritability were not significantly different for this group (t-test  $p = 0.77$ ). **C.** The transcripts with the largest local heritability (top 20) across all four tissues. Local heritability was significantly higher than distal heritability of these genes (t-test  $p < 2.2^{-16}$ )

252 **Tissue-specific transcriptional programs were associated with metabolic traits**

253 Clustering of transcripts with top loadings in each tissue showed tissue-specific functional modules associated  
254 with obesity and insulin resistance (Fig. 6A) (Methods). The clustering highlights the importance of immune  
255 activation particularly in adipose tissue. The “mitosis” cluster had large positive loadings in three of the four  
256 tissues potentially suggesting system-wide proliferation of immune cells. Otherwise, all clusters were strongly  
257 loaded in only one or two tissues. For example, the lipid metabolism cluster was loaded most heavily in liver.  
258 The positive loadings suggest that high expression of these genes, particularly in the liver, was associated with  
259 increased metabolic disease. This cluster included the gene *Pparg*, whose primary role is in the adipose tissue  
260 where it is considered a master regulator of adipogenesis<sup>49</sup>. Agonists of *Pparg*, such as thiazolidinediones, are  
261 FDA-approved to treat type II diabetes, and reduce inflammation and adipose hypertrophy<sup>49</sup>. Consistent  
262 with this role, the loading for *Pparg* in adipose tissue was negative, suggesting that higher expression was  
263 associated with leaner mice (Fig. 6B). In contrast, *Pparg* had a large positive loading in liver, where it is  
264 known to play a role in the development of hepatic steatosis, or fatty liver. Mice that lack *Pparg* specifically  
265 in the liver, are protected from developing steatosis and show reduced expression of lipogenic genes<sup>50;51</sup>.  
266 Overexpression of *Pparg* in the livers of mice with a *Ppara* knockout, causes upregulation of genes involved in  
267 adipogenesis<sup>52</sup>. In the livers of both mice and humans high *Pparg* expression is associated with hepatocytes  
268 that accumulate large lipid droplets and have gene expression profiles similar to that of adipocytes<sup>53;54</sup>.  
269 The local and distal heritability of *Pparg* is low in adipose tissue suggesting its expression in this tissue is  
270 highly constrained in the population (Fig. 6B). However, the distal heritability of *Pparg* in liver is relatively  
271 high suggesting it is complexly regulated and has sufficient variation in this population to drive variation in  
272 phenotype. Both local and distal heritability of *Pparg* in the islet are relatively high, but the loading is low,  
273 suggesting that variability of expression in the islet does not drive variation in MDI. These results highlight  
274 the importance of tissue context when investigating the role of heritable transcript variability in driving  
275 phenotype. Gene lists for all clusters are available in Supp. File 1.

276 **Gene expression, but not local eQTLs, predicted body weight in an independent population**

277 To test whether the transcript loadings identified in the DO could be translated to another population, we  
278 tested whether they could predict metabolic phenotypes in an independent population of CC-RIX mice, which  
279 were F1 mice derived from multiple pairings of Collaborative Cross (CC)<sup>55;32;56;57</sup> strains (Fig. 7) (Methods).  
280 We tested two questions. First, we asked whether the loadings identified in the DO mice were relevant to  
281 the relationship between the transcriptome and the phenotype in the CC-RIX. We predicted body weight  
282 (a surrogate for MDI) in each CC-RIX individual using measured gene expression in each tissue and the

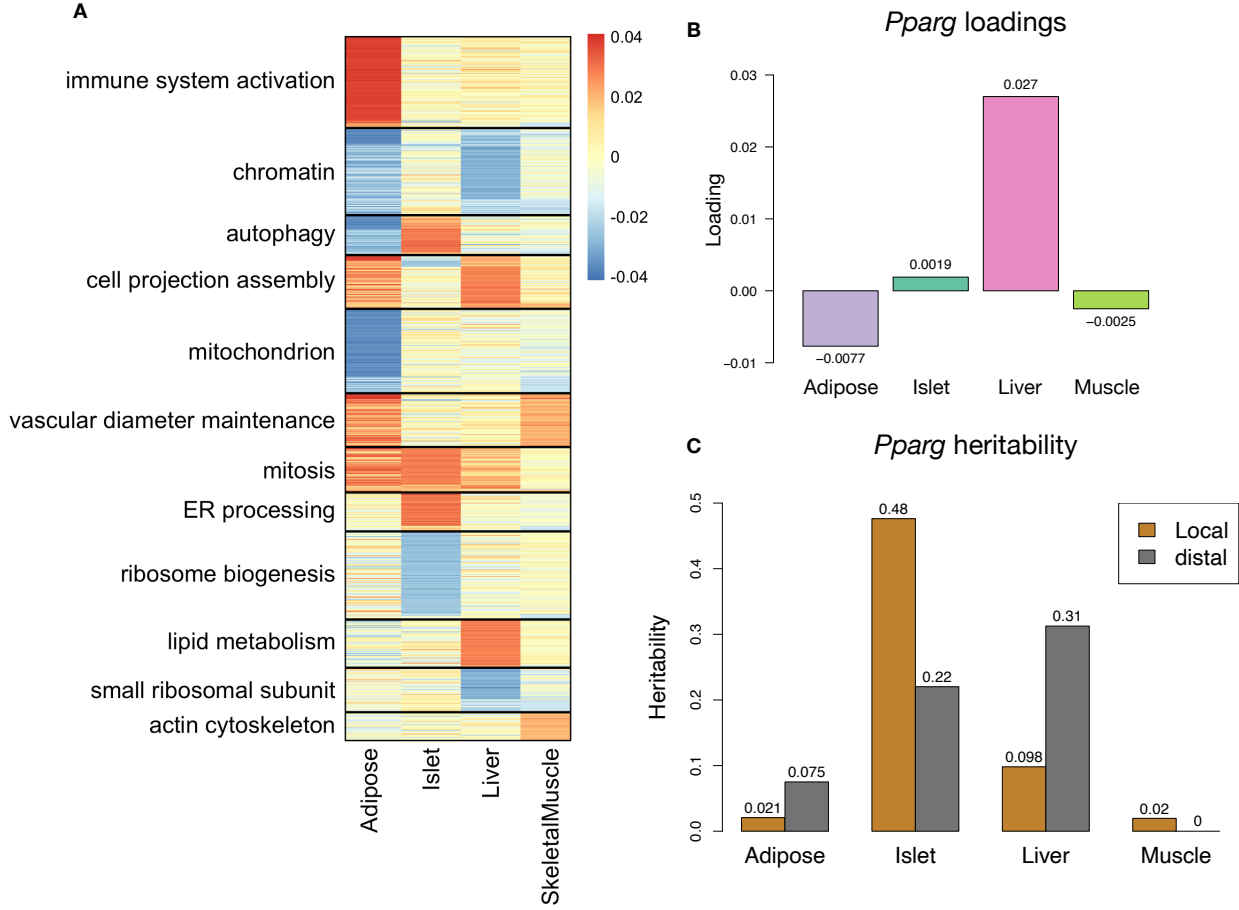


Figure 6: Tissue-specific transcriptional programs were associated with obesity and insulin resistance. **A** Heat map showing the loadings of all transcripts with loadings greater than 2.5 standard deviations from the mean in any tissue. The heat map was clustered using k medoid clustering. Functional enrichments of each cluster are indicated along the left margin. **B** Loadings for *Pparg* in different tissues. **C** Local and distal of *Pparg* expression in different tissues.

283 transcript loadings identified in the DO (Methods). The predicted body weight and acutal body weight were  
 284 highly correlated (Fig. 7B left column). The best prediction was achieved for adipose tissue, which supports  
 285 the observation in the DO that adipose expression was the strongest mediator of the genetic effect on MDI.  
 286 This result also confirms the validity and translatability of the transcript loadings and their relationship to  
 287 metabolic disease.

288 The second question related to the source of the relevant variation in gene expression. If local regulation was  
 289 the predominant factor influencing trait-relevant gene expression, we should be able to predict phenotype in  
 290 the CC-RIX using transcripts imputed from local genotype (Fig. 7A). The DO and the CC-RIX were derived  
 291 from the same eight founder strains and so carry the same alleles throughout the genome. We imputed gene  
 292 expression in the CC-RIX using local genotype and were able to estimate variation in gene transcription

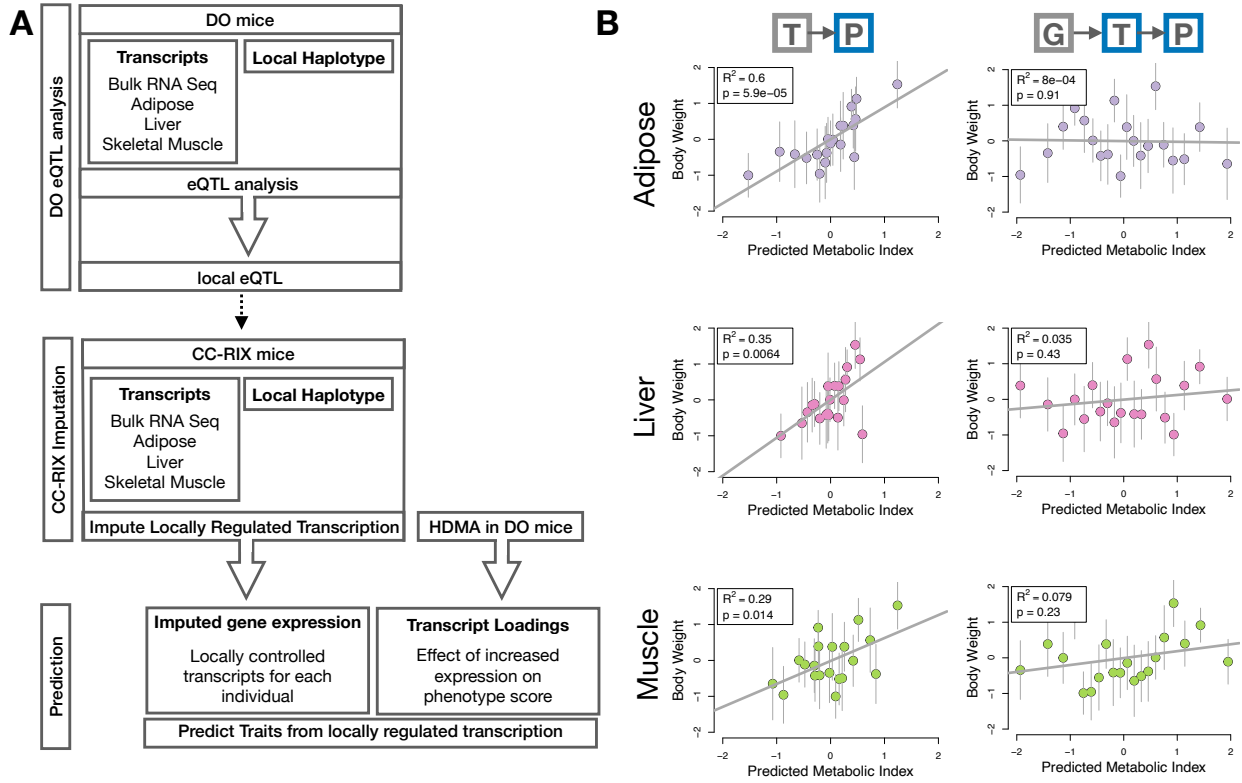


Figure 7: Transcription, but not local genotype, predicts phenotype in the CC-RIX. **A.** Workflow showing procedure for translating HDMA results to an independent population of mice. **B.** Relationships between the predicted metabolic disease index (MDI) and measured body weight in the CC-RIX. The left column shows the predictions using measured transcripts. The right column shows the prediction using transcript levels imputed from local genotype. Gray boxes indicate measured quantities, and blue boxes indicate calculated quantities. The dots in each panel represent individual CC-RIX strains. The gray lines show the standard deviation on body weight for the strain.

robustly (Supp. Fig. S9). However, these imputed values failed to predict body weight in the CC-RIX when weighted with the loadings from HDMA. (Fig. 7B right column). This result suggests that local regulation of gene expression is not the primary factor driving heritability of complex traits. It is also consistent with our findings in the DO population that distal heritability was a major driver of trait-relevant gene expression and that high-loading transcripts had comparatively high distal and low local heritability.

## 298 Distally heritable transcriptomic signatures reflected variation in composition of adipose tissue 299 and islets

The interpretation of global genetic influences on gene expression and phenotype is potentially more challenging than the interpretation and translation of local genetic influences, as genetic effects cannot be localized to individual gene variants or transcripts. However, there are global patterns across the loadings that can inform mechanism. For example, heritable variation in cell type composition can be inferred from transcript loadings.

304 We observed above that immune activation in the adipose tissue was a highly enriched process correlating  
 305 with obesity in the DO population. In humans, it has been extensively observed that macrophage infiltration  
 306 in adipose tissue is a marker of obesity and metabolic disease<sup>58</sup>. To determine whether the immune activation  
 307 reflected a heritable change in cell composition in adipose tissue in DO mice, we compared loadings of  
 308 cell-type specific genes in adipose tissue (Methods). The mean loading of macrophage-specific genes was  
 309 significantly greater than 0 (Holm-adjusted two-sided empirical  $p < 2 \times 10^{-16}$ ) (Fig. 8A), indicating that  
 310 obese mice were genetically predisposed to have high levels of macrophage infiltration in adipose tissue in  
 311 response to the HFHS diet. Loadings for marker genes for other cell types were not statistically different  
 312 from zero (Adipocytes:  $p = 0.08$ , Progenitors:  $p = 0.58$ , Leukocytes:  $p = 0.28$ ; all Holm-adjusted two-sided  
 313 empirical  $p$ ), indicating that changes in the abundance of those cell types was not a mediator of MDI.

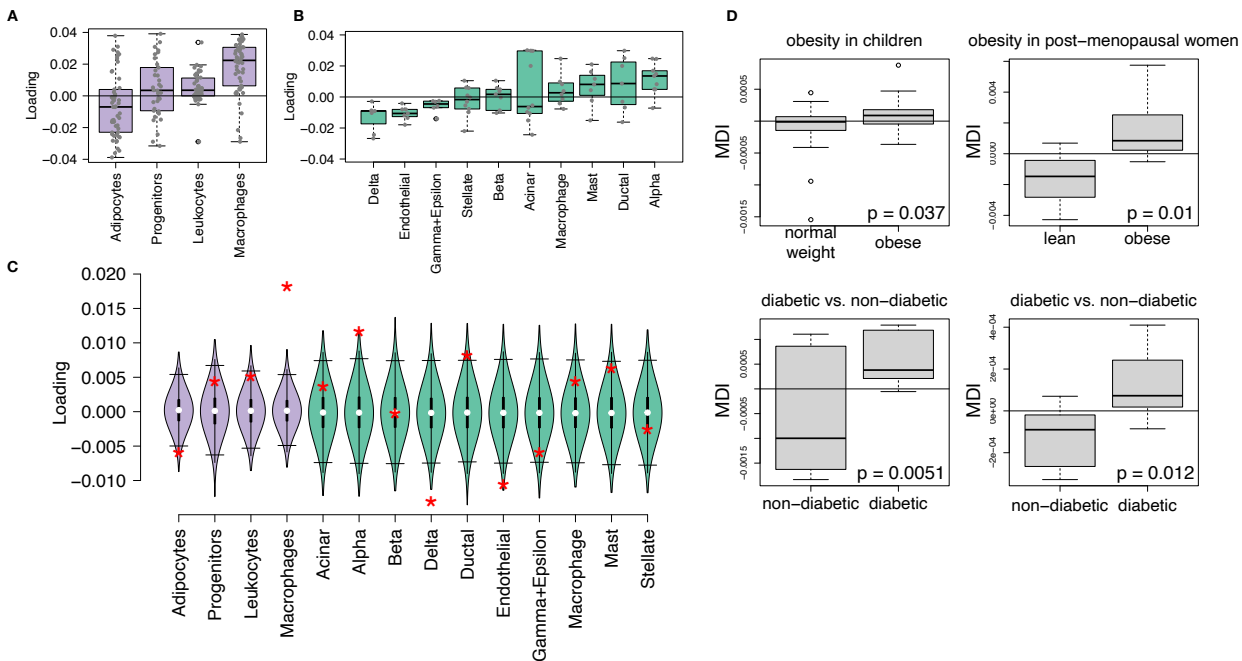


Figure 8: HDMA results translate to humans. **A.** Distribution of loadings for cell-type-specific transcripts in adipose tissue. **B.** Distribution of loadings for cell-type-specific transcripts in pancreatic islets. **C.** Null distributions for the mean loading of randomly selected transcripts in each cell type compared with the observed mean loading of each group of transcripts (red asterisk). **D.** Predictions of metabolic phenotypes in four adipose transcription data sets downloaded from GEO. In each study the obese/diabetic patients were predicted to have greater MDI than the lean/non-diabetic patients based on the HDMA results from DO mice.

314 We also compared loadings of cell-type specific transcripts in islet (Methods). The mean loadings for alpha-cell  
 315 specific transcripts were significantly greater than 0 ( $p = 0.002$ ), while the mean loadings for delta- (Holm-  
 316 adjusted two-sided empirical  $p < 2 \times 10^{-16}$ ) and endothelial-cell (Holm-adjusted two-sided empirical  $p = 0.01$ )  
 317 specific genes were significantly less than 0 (Fig. 8B). These results suggest that mice with higher MDI

318 inherited an altered cell composition that predisposed them to metabolic disease, or that these compositional  
319 changes were induced by the HFHS diet in a heritable way. In either case, these results support the hypothesis  
320 that alterations in islet composition drive variation in MDI. Notably, the mean loading for pancreatic beta  
321 cell marker transcripts was not significantly different from zero (Holm-adjusted two-sided empirical  $p = 0.95$ ).  
322 We stress that this is not necessarily reflective of the function of the beta cells in the obese mice, but rather  
323 suggests that any variation in the number of beta cells in these mice was unrelated to obesity and insulin  
324 resistance, the major contributors to MDI. This is further consistent with the islet composition traits having  
325 small loadings in the phenome score (Fig. 4).

### 326 **Heritable transcriptomic signatures translated to human disease**

327 Ultimately, the heritable transcriptomic signatures that we identified in DO mice will be useful if they inform  
328 mechanism and treatment of human disease. To investigate the potential for translation of the gene signatures  
329 identified in DO mice, we compared them to transcriptional profiles in obese and non-obese human subjects  
330 (Methods). We limited our analysis to adipose tissue because the adipose tissue signature had the strongest  
331 relationship to obesity and insulin resistance in the DO.

332 We calculated a predicted MDI for each individual in the human studies based on their adipose tissue gene  
333 expression (Methods) and compared the predicted scores for obese and non-obese groups as well as diabetic  
334 and non-diabetic groups. In all cases, the predicted MDIs were higher on average for individuals in the  
335 obese and diabetic groups compared with the lean and non-diabetic groups (Fig. 8D). This indicates that  
336 the distally heritable signature of MDI identified in DO mice is relevant to obesity and diabetes in human  
337 subjects.

### 338 **Existing therapies are predicted to target mediator gene signatures**

339 Another application of the transcript loading landscape is in ranking potential drug candidates for the  
340 treatment of metabolic disease. Although high-loading transcripts may be good candidates for understanding  
341 specific biology related to obesity, the transcriptome overall is highly interconnected and redundant. The  
342 ConnectivityMap (CMAP) database<sup>59;60</sup> developed by the Broad Institute allows querying thousands of  
343 compounds that reverse or enhance the extreme ends of transcriptomic signatures in multiple different cell  
344 types. By identifying drugs that reverse pathogenic transcriptomic signatures, we can potentially identify  
345 compounds that have favorable effects on gene expression. To test this hypothesis, we queried the CMAP  
346 database through the CLUE online query tool (<https://clue.io/query/>, version 1.1.1.43) (Methods). We  
347 identified top anti-correlated hits across all cell types (Supp. Figs S10 and S11). To get more tissue-specific

348 results, we also looked at top results in cell types that most closely resembled our tissues. We looked at  
349 results in adipocytes (ASC) as well as pancreatic tumor cells (YAPC) regardless of *p* value (Supp. Figs S12  
350 and S13).

351 The CMAP database identified both known diabetes drugs (e.g. sulfonylureas), as well as drugs that target  
352 pathways known to be involved in diabetes pathogenesis (e.g. mTOR inhibitors). These findings help  
353 support the mediation model we fit here. Although the composite variables we identified here are consistent  
354 with mediation, they do not prove causality. However, the results from CMAP suggest that reversing the  
355 transcriptomic signatures we found also reverses metabolic disease phenotypes, which supports a causal role  
356 of the transcript levels in driving pathogenesis of metabolic disease. These results thus support the mediation  
357 model we identified here and its translation to therapies in human disease.

## 358 Discussion

359 Here we investigated the relative contributions of local and distal gene regulation in four tissues to heritable  
360 variation in traits related to metabolic disease in genetically diverse mice. We found that distal heritability  
361 was positively correlated with trait relatedness, whereas high local heritability was negatively correlated with  
362 trait relatedness. We used a novel high-dimensional mediation analysis (HDMA) to identify tissue-specific  
363 composite transcripts that are predicted to mediate the effect of genetic background on metabolic traits. The  
364 adipose-derived composite transcript robustly predicted body weight in an independent cohort of diverse  
365 mice with disparate population structure. It also predicted MDI in four human cohorts. However, gene  
366 expression imputed from local genotype failed to predict body weight in the second mouse population. Taken  
367 together, these results highlight the complexity of gene expression regulation in relation to trait heritability  
368 and suggest that heritable trait variation is mediated primarily through distal gene regulation.

369 Our result that distal regulation accounted for most trait-related gene expression differences is consistent  
370 with a complex model of genetic trait determination. It has frequently been assumed that gene regulation in  
371 *cis* is the primary driver of genetically associated trait variation, but attempts to use local gene regulation  
372 to explain phenotypic variation have had limited success<sup>16;17</sup>. In recent years, evidence has mounted that  
373 distal gene regulation may be an important mediator of trait heritability<sup>19;18;61;62</sup>. It has been observed  
374 that transcripts with high local heritability explain less expression-mediated disease heritability than those  
375 with low local heritability<sup>19</sup>. Consistent with this observation, genes located near GWAS hits tend to be  
376 complexly regulated<sup>18</sup>. They also tend to be enriched with functional annotations, in contrast to genes with  
377 simple local regulation, which tend to be depleted of functional annotations suggesting they are less likely  
378 to be directly involved in disease traits<sup>18</sup>. These observations are consistent with principles of robustness

379 in complex systems in which simple regulation of important elements leads to fragility of the system<sup>63–65</sup>.  
380 Our results are consistent, instead, with a more complex picture where genes whose expression can drive  
381 trait variation are buffered from local genetic variation but are extensively influenced indirectly by genetic  
382 variation in the regulatory networks converging on those genes.

383 Our results are also consistent with the recently proposed omnigenic model, which posits that complex traits  
384 are massively polygenic and that their heritability is spread out across the genome<sup>66</sup>. In the omnigenic model,  
385 genes are classified either as “core genes,” which directly impinge on the trait, or “peripheral genes,” which  
386 are not directly trait-related, but influence core genes through the complex gene regulatory network. HDMA  
387 explicitly models a central proposal of the omnigenic model which posits that once the expression of the  
388 core genes (i.e. trait-mediating genes) is accounted for, there should be no residual correlation between the  
389 genome and the phenotype. Here, we were able to fit this model and identified a composite transcript that,  
390 when taken into account, left no residual correlation between the composite genome and composite phenotype  
391 scores (Fig. 3A, Supp. Fig 4E).

392 Unlike in the omnigenic model, we did not observe a clear demarcation between the core and peripheral  
393 genes in loading magnitude, but we do not necessarily expect a clear separation given the complexity of gene  
394 regulation and the genotype-phenotype map<sup>67</sup>.

395 An extension of the omnigenic model proposed that most heritability of complex traits is driven by weak  
396 distal eQTLs that are potentially below the detection threshold in studies with feasible sample sizes<sup>61</sup>. This  
397 is consistent with what we observed here. For example, *Nucb2*, had a high loading in islets and was also  
398 strongly distally regulated (66% distal heritability) (Fig. 5). This gene is expressed in pancreatic  $\beta$  cells and  
399 is involved in insulin and glucagon release<sup>68–70</sup>. Although its transcription was highly heritable in islets, that  
400 regulation was distributed across the genome, with no clear distal eQTL (Supp. Fig. S14). Thus, although  
401 distal regulation of some genes may be strong, this regulation is likely to be highly complex and not easily  
402 localized.

403 Individual high-loading transcripts also demonstrated biologically interpretable, tissue-specific patterns. We  
404 highlighted *Pparg*, which is known to be protective in adipose tissue<sup>49</sup> where it was negatively loaded, and  
405 harmful in the liver<sup>50–54</sup>, where it was positively loaded. Such granular patterns may be useful in generating  
406 hypotheses for further testing, and prioritizing genes as therapeutic targets. The tissue-specific nature of  
407 the loadings also may provide clues to tissue-specific effects, or side effects, of targeting particular genes  
408 system-wide.

409 In addition to identifying individual transcripts of interest, the composite transcripts can be used as weighted

410 vectors in multiple types of analysis, such as drug prioritization using gene set enrichment analysis (GSEA)  
411 and the CMAP database. In particular, the CMAP analysis identified drugs which have been demonstrated  
412 to reverse insulin resistance and other aspects of metabolic disease. This finding supports the hypothesis  
413 that HDMA identified transcripts that truly mediate genetic effects on traits. On its own, HDMA identifies  
414 transcriptional patterns that are consistent with a mediation model, but alone does not prove mediation.  
415 However, the finding that these drugs act both on the transcriptional patterns and on the desired traits  
416 support the mediation model and the hypothesis that these transcripts have a causal role in pathogenesis of  
417 metabolic disease.

418 Together, our results have shown that both tissue specificity and distal gene regulation are critically important  
419 to understanding the genetic architecture of complex traits. We identified important genes and gene signatures  
420 that were heritable, plausibly causal of disease, and translatable to other mouse populations and to humans.  
421 Finally, we have shown that by directly acknowledging the complexity of both gene regulation and the  
422 genotype-to-phenotype map, we can gain a new perspective on disease pathogenesis and develop actionable  
423 hypotheses about pathogenic mechanisms and potential treatments.

## 424 Data and Code Availability

425 **DO mice:** Genotypes, phenotypes, and pancreatic islet gene expression data were previously published<sup>12</sup>.  
426 Gene expression for the other tissues can be found at the Gene Expression Omnibus <https://www.ncbi.nlm.nih.gov/geo/> with the following accession numbers: DO adipose tissue - GSE266549; DO liver tissue  
427 - GSE266569; DO skeletal muscle - GSE266567. Expression data with calculated eQTLs are available at  
428 Figshare [https://figshare.com/articles/dataset/Data\\_and\\_code\\_for\\_High-Dimensional\\_Mediation\\_Analysis\\_HDMA\\_in\\_diversity\\_outbred\\_mice/27066979](https://figshare.com/articles/dataset/Data_and_code_for_High-Dimensional_Mediation_Analysis_HDMA_in_diversity_outbred_mice/27066979) DOI: 10.6084/m9.figshare.27066979  
430  
431 10.6084/m9.figshare.27066979.v1

432 **CC-RIX mice:** Gene expression can be found at the Gene Expression Omnibus <https://www.ncbi.nlm.nih.gov/geo/> with the following accession numbers: CC-RIX adipose tissue - GSE237737; CC-RIX liver tissue -  
433 GSE237743; CC-RIX skeletal muscle - GSE237747. Count matrices and phenotype data can be found at  
434 Figshare [https://figshare.com/articles/dataset/Data\\_and\\_code\\_for\\_High-Dimensional\\_Mediation\\_Analysis\\_HDMA\\_in\\_diversity\\_outbred\\_mice/27066979](https://figshare.com/articles/dataset/Data_and_code_for_High-Dimensional_Mediation_Analysis_HDMA_in_diversity_outbred_mice/27066979) DOI: 10.6084/m9.figshare.27066979  
436

437 **Code:** All code used to run the analyses reported here are available at Figshare: [https://figshare.com/articles/dataset/Data\\_and\\_code\\_for\\_High-Dimensional\\_Mediation\\_Analysis\\_HDMA\\_in\\_diversity\\_outbred\\_mice/27066979](https://figshare.com/articles/dataset/Data_and_code_for_High-Dimensional_Mediation_Analysis_HDMA_in_diversity_outbred_mice/27066979) DOI: 10.6084/m9.figshare.27066979  
439

<sup>440</sup> **Acknowledgements**

<sup>441</sup> This project was supported by The Jackson Laboratory Cube Initiative, as well as grants from the National  
<sup>442</sup> Institutes of Health (grant numbers.: R01DK101573, R01DK102948, and RC2DK125961) (to A. D. A.) and  
<sup>443</sup> by the University of Wisconsin-Madison, Department of Biochemistry and Office of the Vice Chancellor for  
<sup>444</sup> Research and Graduate Education with funding from the Wisconsin Alumni Research Foundation (to M. P.  
<sup>445</sup> K.).

<sup>446</sup> We thank the following scientific services at The Jackson Laboratory: Genome Technologies for the RNA  
<sup>447</sup> sequencing, necropsy services for the tissue harvests, and the Center for Biometric Analysis for metabolic  
<sup>448</sup> phenotyping.

449 **Supplemental Figures**

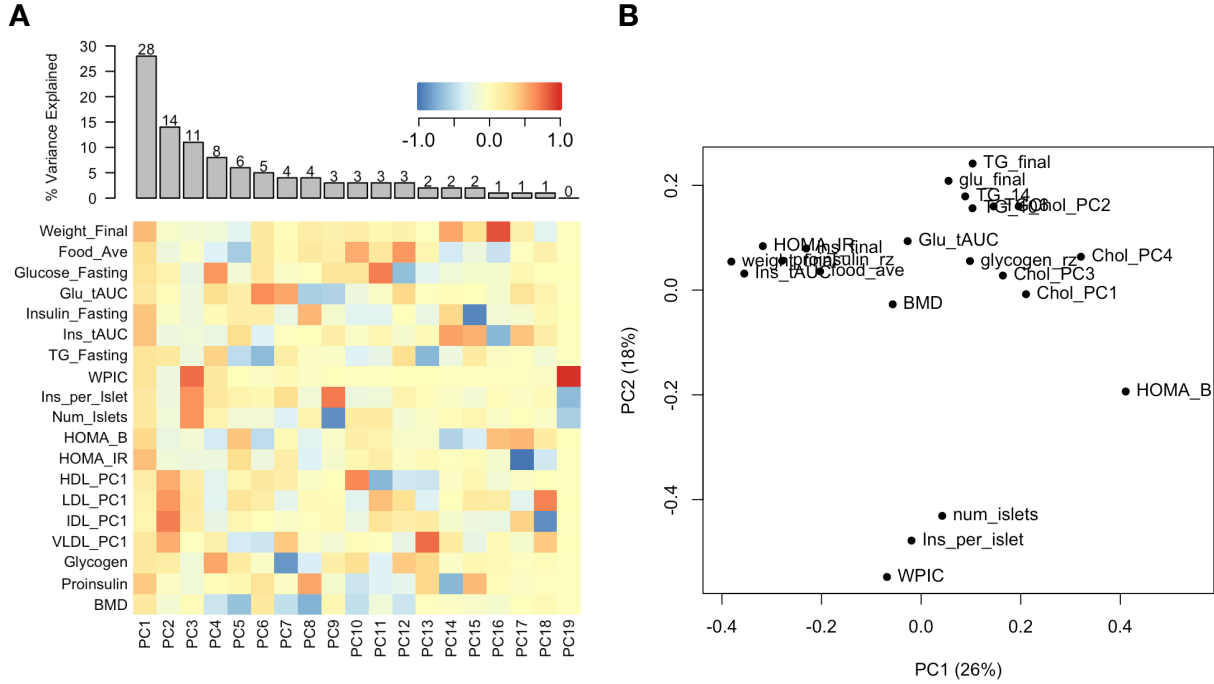


Figure S1: Trait matrix decomposition. **A** The heat map shows the loadings of each trait onto each principal component of the trait matrix. The bars at the top show the percent variance explained for each principal component. **B** Traits plotted by the first and second principal components of the trait matrix. This view shows clustering of traits into insulin- and weight-related traits, lipid-related traits, and ex-vivo pancreatic measurements.

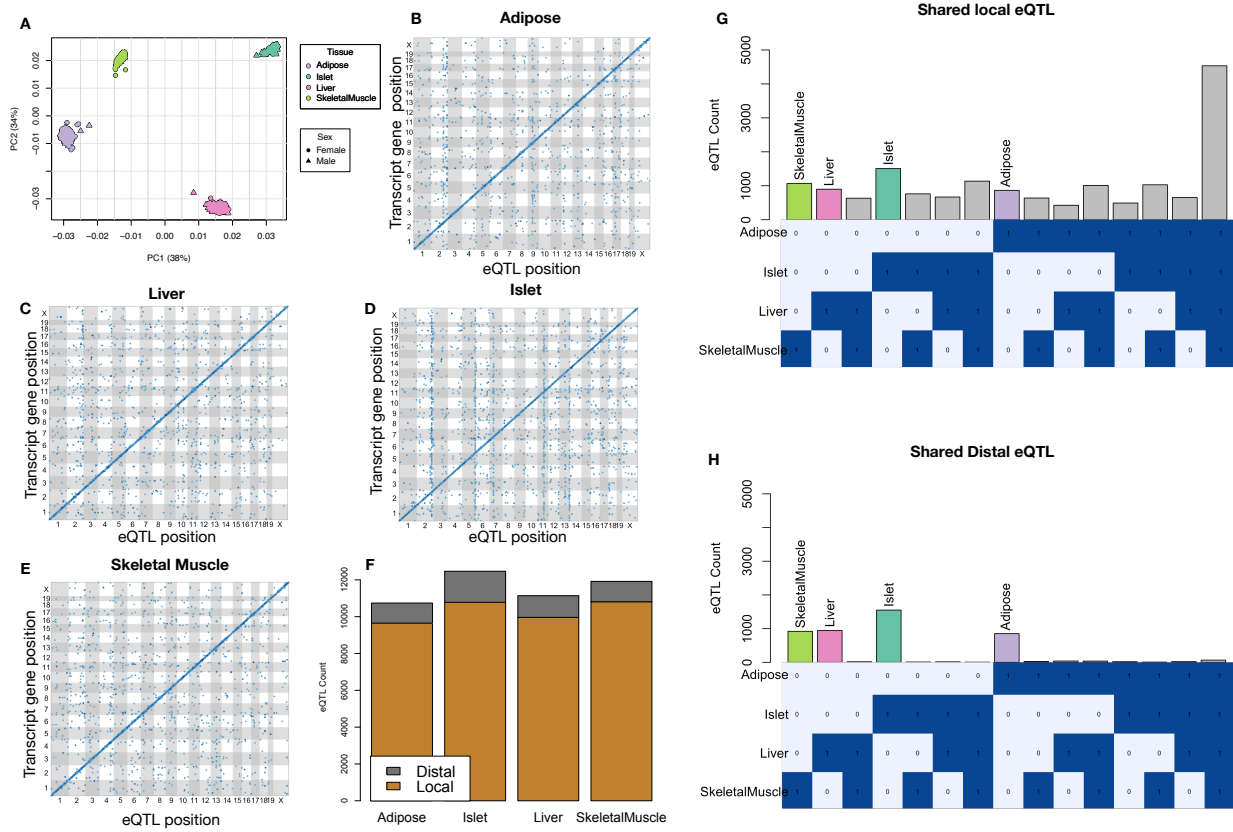


Figure S2: Overview of eQTL analysis in DO mice. **A.** RNA seq samples from the four different tissues clustered by tissue. **B.-E.** eQTL maps are shown for each tissue. The *x*-axis shows the position of the mapped eQTL, and the *y*-axis shows the physical position of the gene encoding each mapped transcript. Each dot represents an eQTL with a minimum LOD score of 8, which represents a genome-wide permutation-based threshold of  $p < 0.01$ . The dots on the diagonal are locally regulated eQTL for which the mapped eQTL is at the within 4Mb of the encoding gene. Dots off the diagonal are distally regulated eQTL for which the mapped eQTL is distant from the gene encoding the transcript. **F.** Comparison of the total number of local and distal eQTL with a minimum LOD score of 8 in each tissue. All tissues have comparable numbers of eQTL. Local eQTLs are much more numerous than distal eQTL. **G.** Counts of transcripts with local eQTL shared across multiple tissues. The majority of local eQTLs were shared across all four tissues. **H.** Counts of transcripts with distal eQTL shared across multiple tissues. The majority of distal eQTL were tissue-specific and not shared across multiple tissues. For both G and H, eQTL for a given transcript were considered shared in two tissues if they were within 4Mb of each other. Colored bars indicate the counts for individual tissues for easy of visualization.

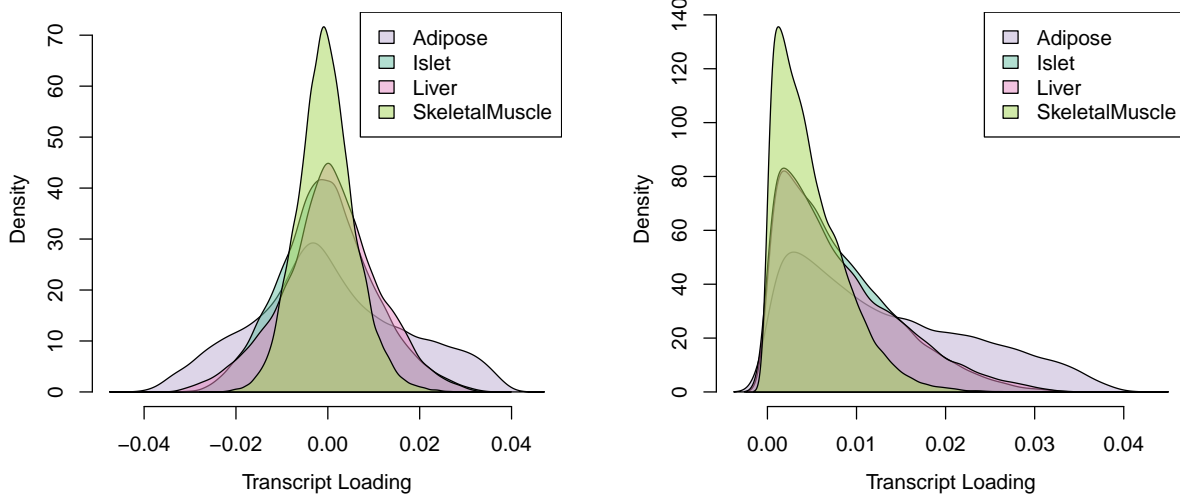


Figure S3: Direct comparisons of transcript loadings across tissues. **A.** Distributions of transcript loadings are shown as density curves and are differentially colored to indicate tissue. Transcripts in adipose tissue had both the largest positive and negative loadings. **B.** Direct comparison of absolute values of transcript loadings across tissues. Transcripts in adipose tissue had the largest loadings overall, while those in skeletal muscle had the smallest.

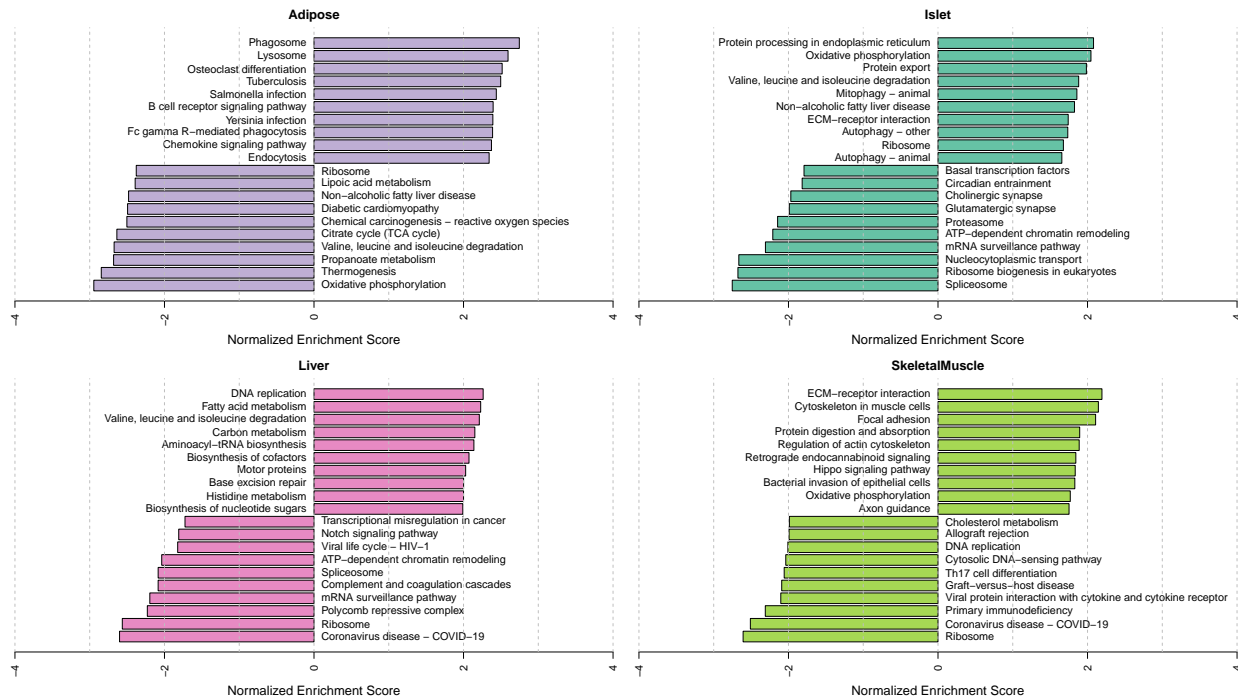


Figure S4: Bar plots showing normalized enrichment scores (NES) for KEGG pathways as determined by fast gene score enrichment analysis (fgsea). Only the top 10 positive and top 10 negative scores are shown. Colors indicate tissue. The name beside each bar shows the name of each enriched KEGG pathway.

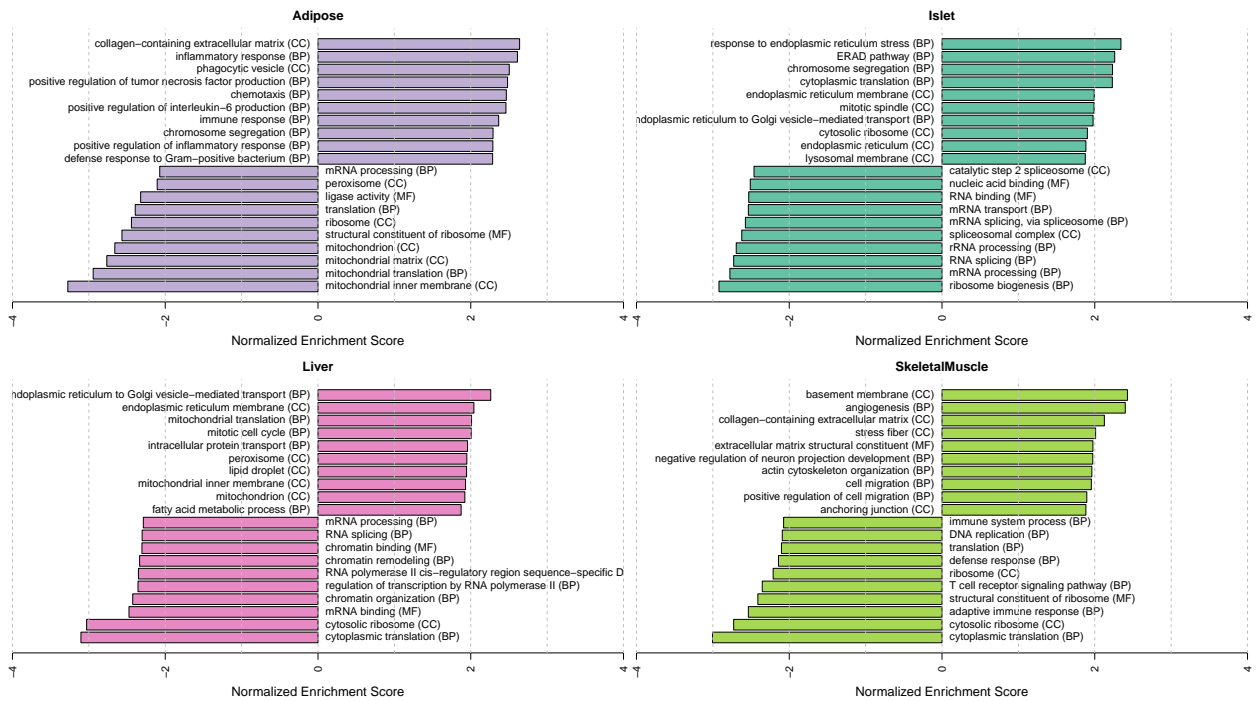


Figure S5: Bar plots showing normalized enrichment scores (NES) for GO terms as determined by fast gene score enrichment analysis (fgsea). Only the top 10 positive and top 10 negative scores are shown. Colors indicate tissue. The name beside each bar shows the name of each enriched GO term. The letters in parentheses indicate whether the term is from the biological process ontology (BP), the molecular function ontology (MF), or the cellular compartment ontology (CC).

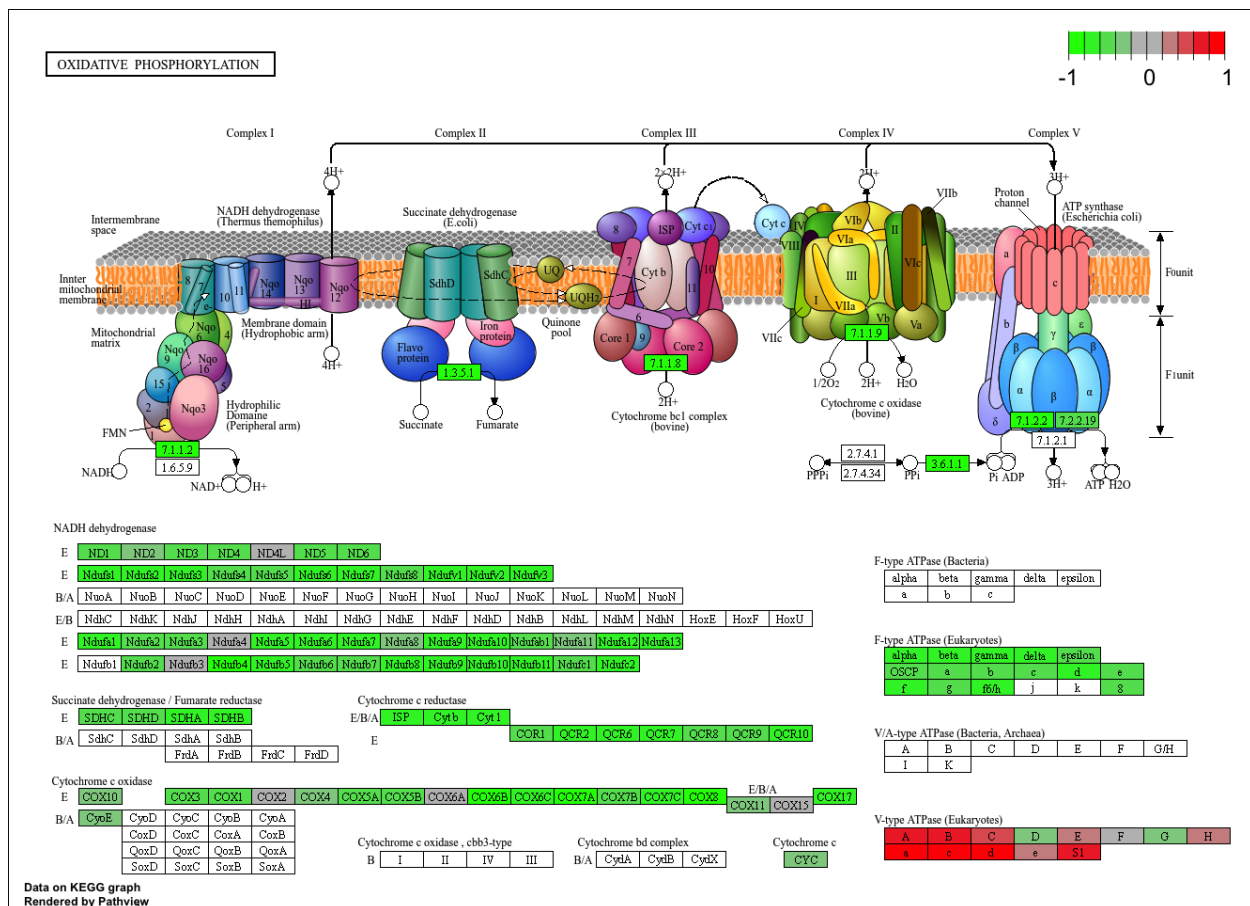


Figure S6: The KEGG pathway for oxidative phosphorylation in mice. Each element is colored based on its HDMA loading from adipose tissue scaled to run from -1 to 1. Genes highlighted in green had negative loadings, and those highlighted in red had positive loadings. Almost the entire pathway was strongly negatively loaded indicating that increased expression of genes involved in oxidative phosphorylation was associated with reduced MDI.

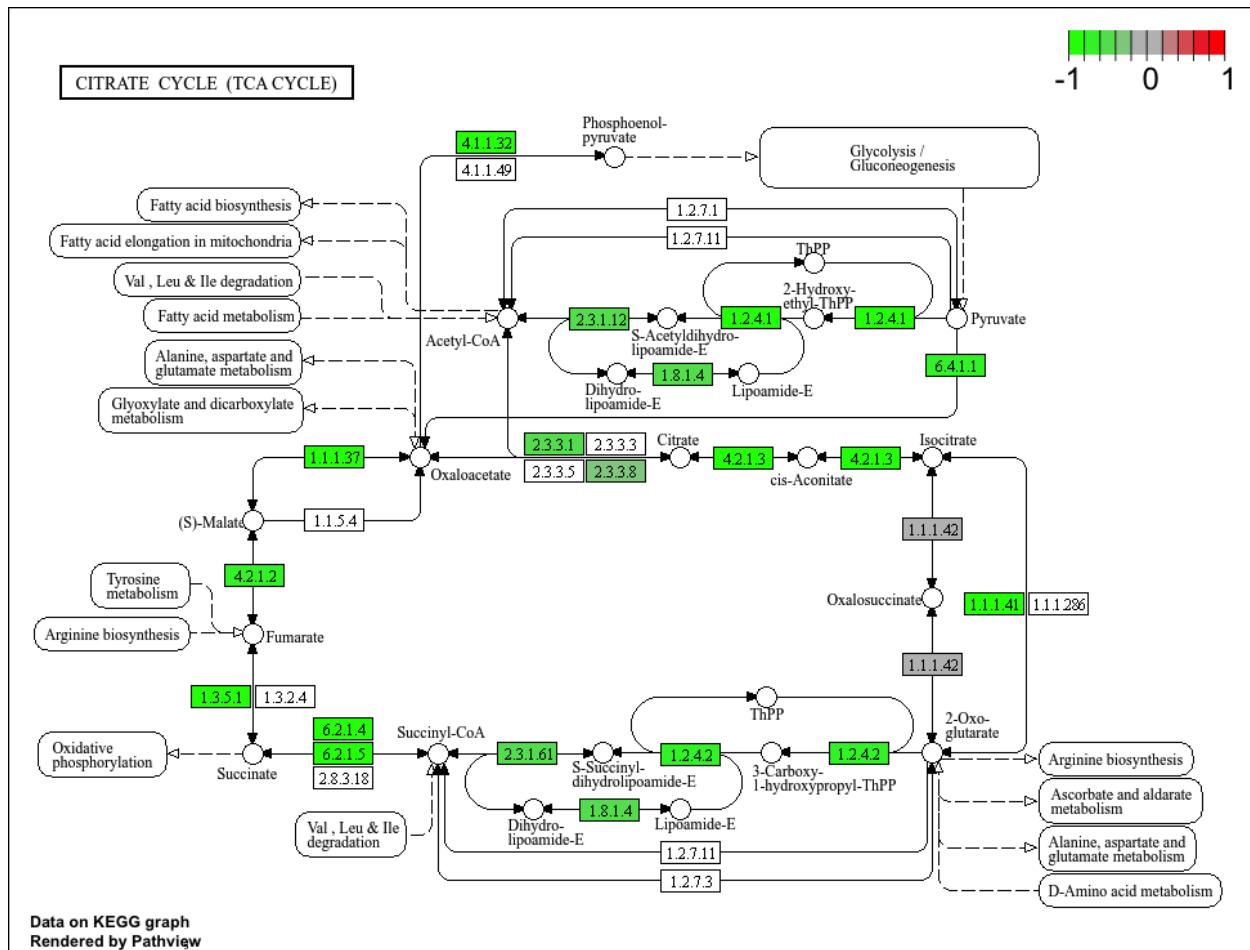


Figure S7: The KEGG pathway for the TCA (citric acid) cycle in mice. Each element is colored based on its HDMA loading from adipose tissue scaled to run from -1 to 1. Genes highlighted in green had negative loadings, and those highlighted in red had positive loadings. Many genes in the cycle were strongly negatively loaded indicating that increased expression of genes involved in the TCA cycle was associated with reduced MDI.

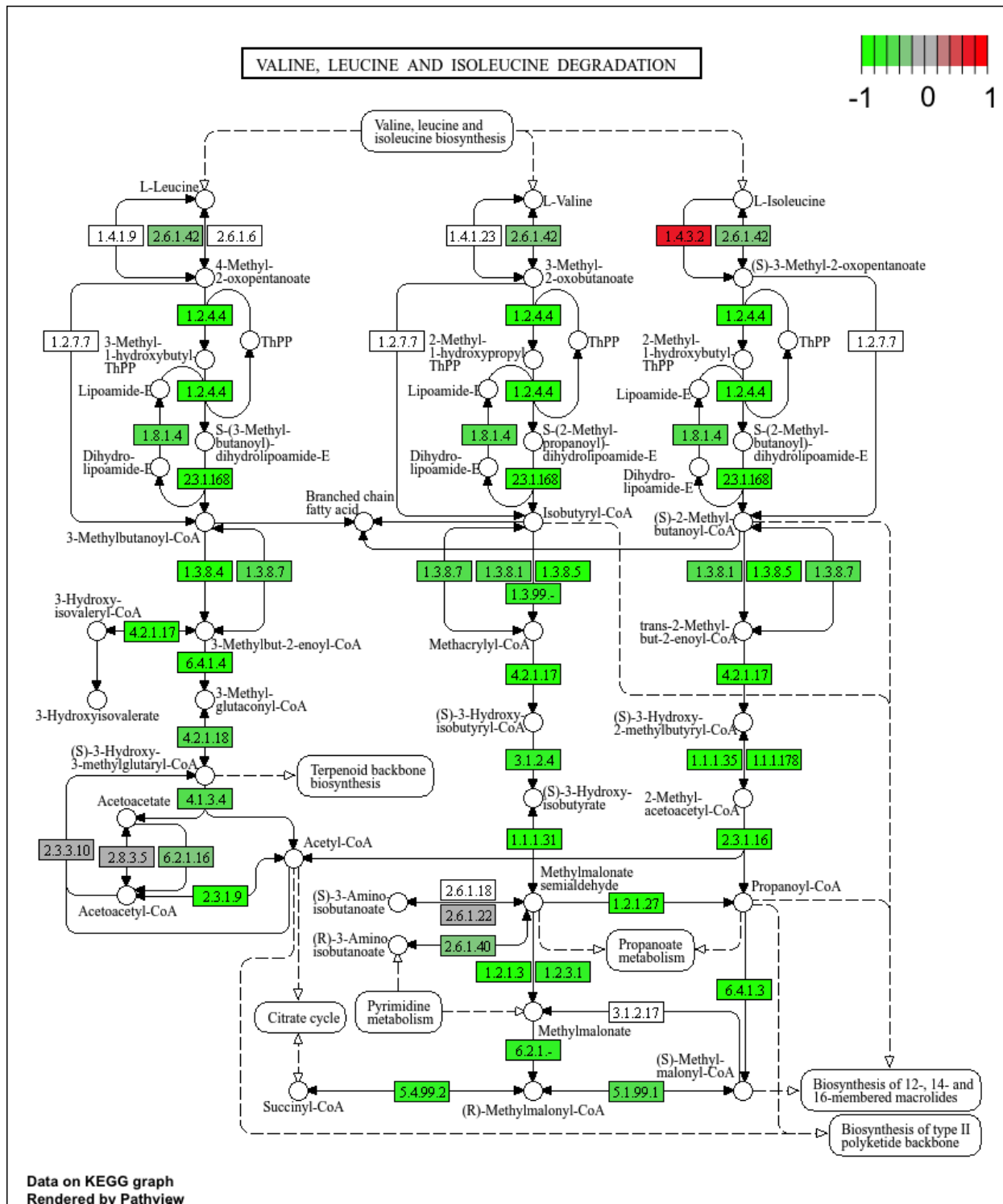


Figure S8: The KEGG pathway for branched-chain amino acid degradation in mice. Each element is colored based on its HDMA loading from adipose tissue scaled to run from -1 to 1. Genes highlighted in green had negative loadings, and those highlighted in red had positive loadings. Almost the entire pathway was strongly negatively loaded indicating that increased expression of genes involved in branched-chain amino acid degradation was associated with reduced MDI.

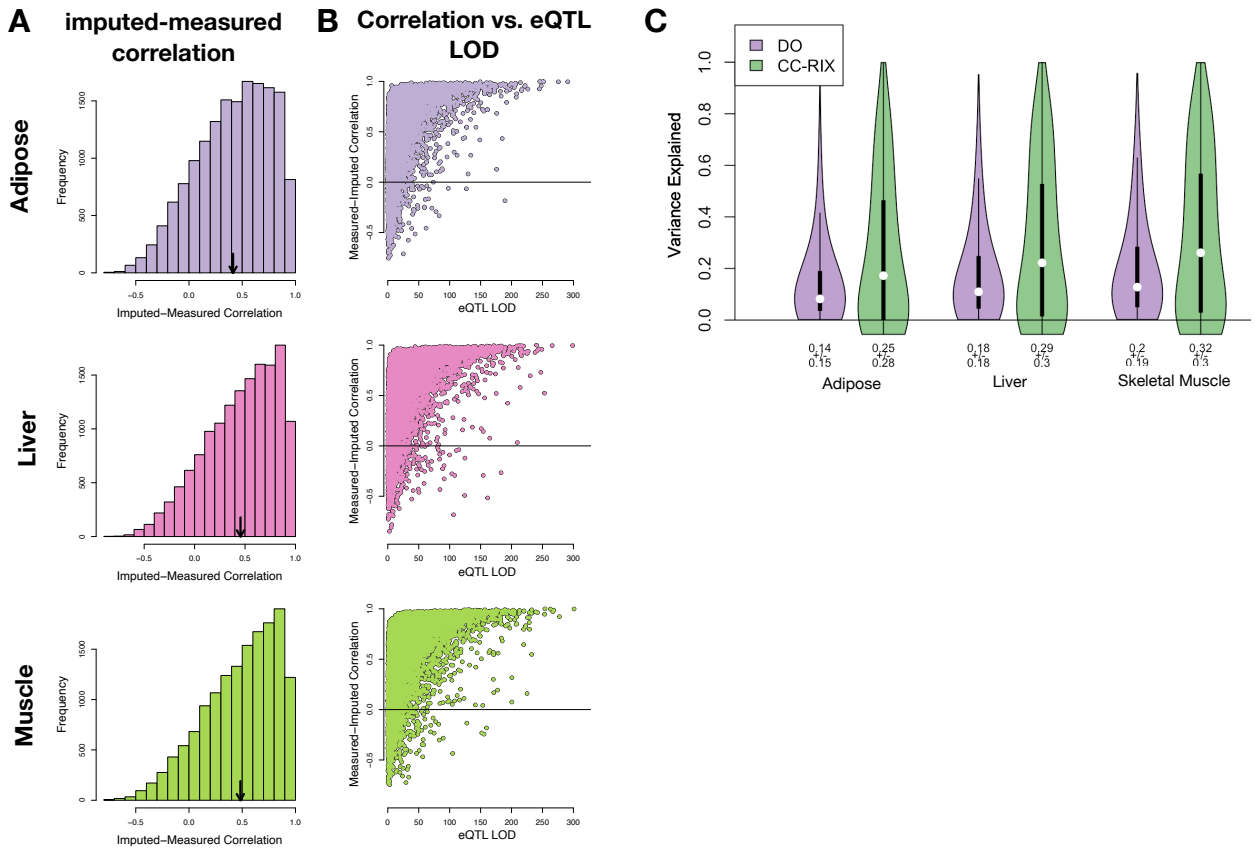


Figure S9: Validation of transcript imputation in the CC-RIX. **A.** Distributions of correlations between imputed and measured transcripts in the CC-RIX. The mean of each distribution is shown by the red line. All distributions were skewed toward positive correlations and had positive means near a Pearson correlation ( $r$ ) of 0.5. **B.** The relationship between the correlation between measured and imputed expression in the CC-RIX (x-axis) and eQTL LOD score. As expected, imputations are more accurate for transcripts with strong local eQTLs. **C.** Distributions of variance explained by local genotype across all transcripts in the DO and CC-RIX.

<b>id</b>	<b>norm_ss</b>	<b>cell_iname</b>	<b>pert_type</b>	<b>raw_ss▲</b>	<b>fdr_q_nlog10</b>	<b>set_type</b>	<b>src_set_id</b>
		HA1E	TRT_CP	-0.97	15.65	PCL	CP_PROTEIN_SYNTHESIS_INHIBITOR
		PC3	TRT_SH.CGS	-0.90	15.65	PATHWAY_SET	BIOCARTA_EIF4_PATHWAY
		A375	TRT_CP	-0.87	15.65	MOA_CLASS	RAF_INHIBITOR
		HCC515	TRT_CP	-0.84	15.65	PCL	CP_TOPOISOMERASE_INHIBITOR
		HEPG2	TRT_SH.CGS	-0.82	15.65	PATHWAY_SET	BIOCARTA_BCR_PATHWAY
		PC3	TRT_CP	-0.77	15.65	MOA_CLASS	MTOR_INHIBITOR
		HCC515	TRT_CP	-0.76	15.65	PCL	CP_GLUCOCORTICOID_RECECTORAGONIST
		HCC515	TRT_CP	-0.76	15.65	MOA_CLASS	GLUCOCORTICOID_RECECTORAGONIST
		A375	TRT_CP	-0.72	15.65	MOA_CLASS	MTOR_INHIBITOR
		-666	TRT_CP	-0.70	15.65	PCL	CP_PROTEIN_SYNTHESIS_INHIBITOR
		-666	TRT_CP	-0.68	15.65	PCL	CP_JAK_INHIBITOR
		A549	TRT_CP	-0.67	15.65	PCL	CP_GLUCOCORTICOID_RECECTORAGONIST
		A549	TRT_CP	-0.67	15.65	MOA_CLASS	GLUCOCORTICOID_RECECTORAGONIST
		-666	TRT_CP	-0.57	15.65	PCL	CP_MTOR_INHIBITOR
		-666	TRT_CP	-0.55	15.65	MOA_CLASS	MTOR_INHIBITOR
		-666	TRT_CP	-0.55	15.65	PCL	CP_PI3K_INHIBITOR
		-666	TRT_CP	0.85	15.65	MOA_CLASS	PKC_ACTIVATOR

Figure S10: CMAP results using the *adipose* tissue composite transcript as an input. Table includes results from *all cell types* sorted with a  $-\log_{10}(q) > 15$ . The results are sorted by the correlation of the query to the input with the most negative results at the top.

id	norm_CS	cell_iname	pert_type	raw_CS▲	fdr_q_nlog10	set_type	src_set_id
		VCAP	TRT_SH.CGS	-0.99	15.65	PATHWAY_SET REACTOME_DOWNSTREAM_TCR_SIGNALING	
		VCAP	TRT_SH.CGS	-0.99	15.65	PATHWAY_SET REACTOME_NOD1_2_SIGNALING_PATHWAY	
		A549	TRT_SH.CGS	-0.92	15.65	PATHWAY_SET BIOCARTA_TNFR1_PATHWAY	
		VCAP	TRT_SH.CGS	-0.92	15.65	PATHWAY_SET HALLMARK_WNT_BETA_CATENIN_SIGNALING	
		HT29	TRT_CP	-0.92	15.65	PCL CP_TUBULIN_INHIBITOR	
-666			TRT_OE	-0.88	15.65	PCL OE_CELL_CYCLE_INHIBITION	
		VCAP	TRT_SH.CGS	-0.87	15.65	PATHWAY_SET REACTOME_P75_NTR_RECECTOR_MEDIATED_SIGNALLING	
		HT29	TRT_CP	-0.86	15.65	MOA_CLASS TUBULIN_INHIBITOR	
		MCF7	TRT_CP	-0.85	15.65	PCL CP_TUBULIN_INHIBITOR	
-666			TRT_CP	-0.81	15.65	PCL CP_PROTEASOME_INHIBITOR	
-666			TRT_SH.CGS	-0.80	15.65	PATHWAY_SET REACTOME_DOWNREGULATION_OF_ERBB2_ERBB3_SIGNALING	
		HCC515	TRT_CP	-0.80	15.65	PCL CP_GLUCOCORTICOID_RECECTORAGONIST	
		HCC515	TRT_CP	-0.80	15.65	MOA_CLASS GLUCOCORTICOID_RECECTORAGONIST	
		A549	TRT_OE	-0.78	15.65	PATHWAY_SET REACTOME_RAF_MAP_KINASE CASCADE	
		A549	TRT_OE	-0.78	15.65	PATHWAY_SET PID_RAS_PATHWAY	
-666			TRT_SH.CGS	-0.78	15.65	PCL KD_RIBOSOMAL_40S_SUBUNIT	
		A549	TRT_OE	-0.76	15.65	PATHWAY_SET REACTOME_SIGNALLING_TO_P38_VIA_RIT_AND_RIN	
		A549	TRT_OE	-0.76	15.65	PATHWAY_SET REACTOME_PROLONGED_ERK_ACTIVATION_EVENTS	
		A549	TRT_OE	-0.73	15.65	PATHWAY_SET PID_TCR_RAS_PATHWAY	
		HA1E	TRT_OE	-0.73	15.65	PATHWAY_SET REACTOME_SHC RELATED_EVENTS	
		HA1E	TRT_OE	-0.71	15.65	PATHWAY_SET PID_EPHB_FWD_PATHWAY	
-666			TRT_CP	-0.70	15.65	MOA_CLASS GLYCOGEN_SYNTHASE_KINASE_INHIBITOR	
		HA1E	TRT_OE	-0.70	15.65	PATHWAY_SET PID_GMCSF_PATHWAY	
		A549	TRT_OE	-0.69	15.65	PATHWAY_SET REACTOME_SIGNALLING_TO_ERKS	
-666			TRT_LIG	-0.69	15.65	PATHWAY_SET PID_ERBB_NETWORK_PATHWAY	
-666			TRT_CP	-0.67	15.65	MOA_CLASS PROTEASOME_INHIBITOR	
-666			TRT_CP	-0.66	15.65	PCL CP_GLYCOGEN_SYNTHASE_KINASE_INHIBITOR	
-666			TRT_CP	0.73	15.65	MOA_CLASS MTOR_INHIBITOR	

Figure S11: CMAP results using the *pancreatic islet* tissue composite transcript as an input. Table includes results from *all cell types* sorted with a  $-\log_{10}(q) > 15$ . The results are sorted by the correlation of the query to the input with the most negative results at the top.

<b>id</b>	<b>norm_ss</b>	<b>cell_iname</b>	<b>pert_type</b>	<b>raw_ss ▲</b>	<b>fdr_q_nlog10</b>	<b>set_type</b>	<b>src_set_id</b>
		ASC	TRT_CP	-0.94	0.79	PCL	CP_PARP_INHIBITOR
		ASC	TRT_CP	-0.94	0.79	MOA_CLASS	PROTEIN_TYROSINE_KINASE_INHIBITOR
		ASC	TRT_CP	-0.84	0.45	MOA_CLASS	BTK_INHIBITOR
		ASC	TRT_CP	-0.81	0.39	MOA_CLASS	LEUCINE_RICH_REPEAT_KINASE_INHIBITOR
		ASC	TRT_CP	-0.81	0.79	PCL	CP_HSP_INHIBITOR
		ASC	TRT_CP	-0.80	0.93	PCL	CP_EGFR_INHIBITOR
		ASC	TRT_CP	-0.79	0.32	MOA_CLASS	T-TYPE_CALCIUM_CHANNEL_BLOCKER
		ASC	TRT_CP	-0.79	1.09	PCL	CP_MTOR_INHIBITOR
		ASC	TRT_CP	-0.76	0.97	PCL	CP_PI3K_INHIBITOR
		ASC	TRT_CP	-0.75	0.20	MOA_CLASS	HISTONE_DEMETHYLASE_INHIBITOR
		ASC	TRT_CP	-0.74	0.42	PCL	CP_IKK_INHIBITOR
		ASC	TRT_CP	-0.74	0.83	PCL	CP_AURORA_KINASE_INHIBITOR
		ASC	TRT_CP	-0.74	0.17	PCL	CP_LEUCINE_RICH_REPEAT_KINASE_INHIBITOR
		ASC	TRT_CP	-0.72	0.36	PCL	CP_BROMODOMAIN_INHIBITOR
		ASC	TRT_CP	-0.71	1.09	MOA_CLASS	TYROSINE_KINASE_INHIBITOR
		ASC	TRT_CP	-0.70	0.82	PCL	CP_PROTEIN_SYNTHESIS_INHIBITOR
		ASC	TRT_CP	-0.67	0.69	PCL	CP_SRC_INHIBITOR
		ASC	TRT_CP	-0.67	0.81	MOA_CLASS	AURORA_KINASE_INHIBITOR
		ASC	TRT_CP	-0.65	0.89	MOA_CLASS	FLT3_INHIBITOR
		ASC	TRT_CP	-0.62	0.40	MOA_CLASS	FGFR_INHIBITOR
		ASC	TRT_CP	-0.59	0.66	MOA_CLASS	MEK_INHIBITOR
		ASC	TRT_CP	-0.59	0.13	MOA_CLASS	SYK_INHIBITOR
		ASC	TRT_CP	-0.58	0.01	PCL	CP_PKC_INHIBITOR
		ASC	TRT_CP	-0.58	0.65	PCL	CP_HDAC_INHIBITOR
		ASC	TRT_CP	-0.58	0.65	PCL	CP_ATPASE_INHIBITOR
		ASC	TRT_CP	-0.53	0.09	PCL	CP_FLT3_INHIBITOR
		ASC	TRT_CP	-0.53	0.42	PCL	CP_P38_MAPK_INHIBITOR
		ASC	TRT_CP	-0.53	0.22	MOA_CLASS	IKK_INHIBITOR
		ASC	TRT_CP	-0.52	0.58	PCL	CP_VEGFR_INHIBITOR
		ASC	TRT_CP	-0.51	-0.00	PCL	CP_T-TYPE_CALCIUM_CHANNEL_BLOCKER

Figure S12: CMAP results using the *adipose* tissue composite transcript as an input. Table includes the top 30 results derived *only from normal adipocytes* (ASC) regardless of significance. The results are sorted by the correlation of the query to the input with the most negative results at the top.

id	norm_CS	cell_iname	pert_type	raw_CS	fdr_q_nlog10	set_type	src_set_id
		YAPC	TRT_CP	-1.00	0.67	MOA_CLASS	ABL_KINASE_INHIBITOR
		YAPC	TRT_CP	-0.99	0.66	PCL	CP_CDK_INHIBITOR
		YAPC	TRT_CP	-0.97	1.41	PCL	CP_TOPOISOMERASE_INHIBITOR
		YAPC	TRT_CP	-0.95	0.70	MOA_CLASS	THYMIDYLATE_SYNTHASE_INHIBITOR
		YAPC	TRT_CP	-0.95	0.62	MOA_CLASS	ADRENERGIC_INHIBITOR
		YAPC	TRT_CP	-0.94	0.50	MOA_CLASS	BENZODIAZEPINE_RECECTOR_ANTAGONIST
		YAPC	TRT_CP	-0.89	0.63	PCL	CP_RIBONUCLEOTIDE_REDUCTASE_INHIBITOR
		YAPC	TRT_CP	-0.88	0.52	MOA_CLASS	VASOPRESSIN_RECECTOR_ANTAGONIST
		YAPC	TRT_CP	-0.85	0.63	MOA_CLASS	ANGIOTENSIN_RECECTOR_ANTAGONIST
		YAPC	TRT_CP	-0.85	0.33	PCL	CP_CANNABINOID_RECECTORAGONIST
		YAPC	TRT_CP	-0.84	0.30	PCL	CP_RETINOID_RECECTORAGONIST
		YAPC	TRT_CP	-0.83	1.19	MOA_CLASS	NFKB_PATHWAY_INHIBITOR
		YAPC	TRT_CP	-0.83	0.54	MOA_CLASS	DNA_ALKYLATING_DRUG
		YAPC	TRT_CP	-0.80	0.50	MOA_CLASS	CHOLESTEROL_INHIBITOR
		YAPC	TRT_CP	-0.79	0.15	MOA_CLASS	SULFONYLUREA
		YAPC	TRT_CP	-0.78	0.52	MOA_CLASS	HIV_INTEGRASE_INHIBITOR
		YAPC	TRT_CP	-0.78	0.13	MOA_CLASS	LEUKOTRIENE_INHIBITOR
		YAPC	TRT_CP	-0.78	0.45	PCL	CP_PPAR_RECECTORAGONIST
		YAPC	TRT_CP	-0.78	0.54	MOA_CLASS	INSULIN_SENSITIZER
		YAPC	TRT_CP	-0.77	0.51	MOA_CLASS	ESTROGEN_RECECTOR_ANTAGONIST
		YAPC	TRT_CP	-0.77	0.76	MOA_CLASS	DNA_SYNTHESIS_INHIBITOR
		YAPC	TRT_XPR	-0.77	0.67	PATHWAY_SET	BIOCARTA_PARKIN_PATHWAY
		YAPC	TRT_CP	-0.77	0.51	PCL	CP_VEGFR_INHIBITOR
		YAPC	TRT_CP	-0.75	0.39	MOA_CLASS	RNA_SYNTHESIS_INHIBITOR
		YAPC	TRT_CP	-0.72	0.60	MOA_CLASS	BCR-ABL_KINASE_INHIBITOR
		YAPC	TRT_XPR	-0.71	0.66	PATHWAY_SET	BIOCARTA_EIF_PATHWAY
		YAPC	TRT_XPR	-0.69	0.54	PATHWAY_SET	PID_CIRCADIAN_PATHWAY
		YAPC	TRT_CP	-0.68	0.77	MOA_CLASS	TOPOISOMERASE_INHIBITOR
		YAPC	TRT_XPR	-0.64	0.49	PATHWAY_SET	BIOCARTA_CBL_PATHWAY
		YAPC	TRT_CP	-0.64	0.53	MOA_CLASS	TUBULIN_INHIBITOR

Figure S13: CMAP results using the *pancreatic islet* composite transcript as an input. Table includes the top 30 results derived *only from YAPC cells*, which are derived from pancreatic carcinoma cells. Results are shown regardless of significance and are sorted by the correlation of the query to the input with the most negative results at the top.

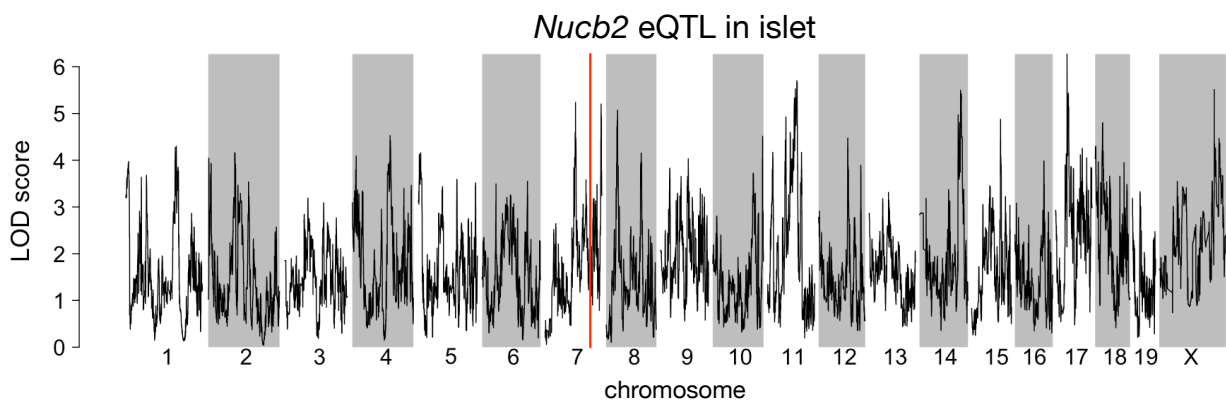


Figure S14: Regulation of *Nucb2* expression in islet. *Nucb2* is encoded on mouse chromosome 7 at 116.5 Mb (red line). In islets the heritability of *Nucb2* expression levels is 69% heritable. This LOD score trace shows that there is no local eQTL at the position of the gene, nor any strong distal eQTLs anywhere else in the genome.

450 **References**

- 451 [1] M. T. Maurano, R. Humbert, E. Rynes, R. E. Thurman, E. Haugen, H. Wang, A. P. Reynolds,  
452 R. Sandstrom, H. Qu, J. Brody, A. Shafer, F. Neri, K. Lee, T. Kutyavin, S. Stehling-Sun, A. K.  
453 Johnson, T. K. Canfield, E. Giste, M. Diegel, D. Bates, R. S. Hansen, S. Neph, P. J. Sabo, S. Heimfeld,  
454 A. Raubitschek, S. Ziegler, C. Cotsapas, N. Sotoodehnia, I. Glass, S. R. Sunyaev, R. Kaul, and J. A.  
455 Stamatoyannopoulos. Systematic localization of common disease-associated variation in regulatory DNA.  
456 *Science*, 337(6099):1190–1195, Sep 2012.
- 457 [2] K. K. Farh, A. Marson, J. Zhu, M. Kleinewietfeld, W. J. Housley, S. Beik, N. Shores, H. Whitton, R. J.  
458 Ryan, A. A. Shishkin, M. Hatan, M. J. Carrasco-Alfonso, D. Mayer, C. J. Luckey, N. A. Patsopoulos,  
459 P. L. De Jager, V. K. Kuchroo, C. B. Epstein, M. J. Daly, D. A. Hafler, and B. E. Bernstein. Genetic  
460 and epigenetic fine mapping of causal autoimmune disease variants. *Nature*, 518(7539):337–343, Feb  
461 2015.
- 462 [3] E. Pennisi. The Biology of Genomes. Disease risk links to gene regulation. *Science*, 332(6033):1031, May  
463 2011.
- 464 [4] L. A. Hindorff, P. Sethupathy, H. A. Junkins, E. M. Ramos, J. P. Mehta, F. S. Collins, and T. A. Manolio.  
465 Potential etiologic and functional implications of genome-wide association loci for human diseases and  
466 traits. *Proc Natl Acad Sci*, 106(23):9362–9367, Jun 2009.
- 467 [5] J. K. Pickrell. Joint analysis of functional genomic data and genome-wide association studies of 18  
468 human traits. *Am J Hum Genet*, 94(4):559–573, Apr 2014.
- 469 [6] D. Welter, J. MacArthur, J. Morales, T. Burdett, P. Hall, H. Junkins, A. Klemm, P. Flieck, T. Manolio,  
470 L. Hindorff, and H. Parkinson. The NHGRI GWAS Catalog, a curated resource of SNP-trait associations.  
471 *Nucleic Acids Res*, 42(Database issue):D1001–1006, Jan 2014.
- 472 [7] Y. I. Li, B. van de Geijn, A. Raj, D. A. Knowles, A. A. Petti, D. Golan, Y. Gilad, and J. K. Pritchard.  
473 RNA splicing is a primary link between genetic variation and disease. *Science*, 352(6285):600–604, Apr  
474 2016.
- 475 [8] D. Zhou, Y. Jiang, X. Zhong, N. J. Cox, C. Liu, and E. R. Gamazon. A unified framework for joint-tissue  
476 transcriptome-wide association and Mendelian randomization analysis. *Nat Genet*, 52(11):1239–1246,  
477 Nov 2020.
- 478 [9] E. R. Gamazon, H. E. Wheeler, K. P. Shah, S. V. Mozaffari, K. Aquino-Michaels, R. J. Carroll, A. E.

- 479        Eyler, J. C. Denny, D. L. Nicolae, N. J. Cox, and H. K. Im. A gene-based association method for  
480        mapping traits using reference transcriptome data. *Nat Genet*, 47(9):1091–1098, Sep 2015.
- 481        [10] Z. Zhu, F. Zhang, H. Hu, A. Bakshi, M. R. Robinson, J. E. Powell, G. W. Montgomery, M. E. Goddard,  
482        N. R. Wray, P. M. Visscher, and J. Yang. Integration of summary data from GWAS and eQTL studies  
483        predicts complex trait gene targets. *Nat Genet*, 48(5):481–487, May 2016.
- 484        [11] A. Gusev, A. Ko, H. Shi, G. Bhatia, W. Chung, B. W. Penninx, R. Jansen, E. J. de Geus, D. I. Boomsma,  
485        F. A. Wright, P. F. Sullivan, E. Nikkola, M. Alvarez, M. Civelek, A. J. Lusis, T. ki, E. Raitoharju,  
486        M. nen, I. ä, O. T. Raitakari, J. Kuusisto, M. Laakso, A. L. Price, P. Pajukanta, and B. Pasaniuc.  
487        Integrative approaches for large-scale transcriptome-wide association studies. *Nat Genet*, 48(3):245–252,  
488        Mar 2016.
- 489        [12] M. P. Keller, D. M. Gatti, K. L. Schueler, M. E. Rabaglia, D. S. Stapleton, P. Simecek, M. Vincent,  
490        S. Allen, A. T. Broman, R. Bacher, C. Kendzierski, K. W. Broman, B. S. Yandell, G. A. Churchill, and  
491        A. D. Attie. Genetic Drivers of Pancreatic Islet Function. *Genetics*, 209(1):335–356, May 2018.
- 492        [13] W. L. Crouse, G. R. Keele, M. S. Gastonguay, G. A. Churchill, and W. Valdar. A Bayesian model  
493        selection approach to mediation analysis. *PLoS Genet*, 18(5):e1010184, May 2022.
- 494        [14] J. M. Chick, S. C. Munger, P. Simecek, E. L. Huttlin, K. Choi, D. M. Gatti, N. Raghupathy, K. L. Svenson,  
495        G. A. Churchill, and S. P. Gygi. Defining the consequences of genetic variation on a proteome-wide scale.  
496        *Nature*, 534(7608):500–505, Jun 2016.
- 497        [15] H. E. Wheeler, S. Ploch, A. N. Barbeira, R. Bonazzola, A. Andaleon, A. Fotuhi Siahpirani, A. Saha,  
498        A. Battle, S. Roy, and H. K. Im. Imputed gene associations identify replicable trans-acting genes enriched  
499        in transcription pathways and complex traits. *Genet Epidemiol*, 43(6):596–608, Sep 2019.
- 500        [16] B. D. Umans, A. Battle, and Y. Gilad. Where Are the Disease-Associated eQTLs? *Trends Genet*,  
501        37(2):109–124, Feb 2021.
- 502        [17] N. J. Connally, S. Nazeen, D. Lee, H. Shi, J. Stamatoyannopoulos, S. Chun, C. Cotsapas, C. A. Cassa,  
503        and S. R. Sunyaev. The missing link between genetic association and regulatory function. *Elife*, 11, Dec  
504        2022.
- 505        [18] H. Mostafavi, J. P. Spence, S. Naqvi, and J. K. Pritchard. Systematic differences in discovery of genetic  
506        effects on gene expression and complex traits. *Nat Genet*, 55(11):1866–1875, Nov 2023.
- 507        [19] D. W. Yao, L. J. O'Connor, A. L. Price, and A. Gusev. Quantifying genetic effects on disease mediated  
508        by assayed gene expression levels. *Nat Genet*, 52(6):626–633, Jun 2020.

- 509 [20] X. Liu, J. A. Mefford, A. Dahl, Y. He, M. Subramaniam, A. Battle, A. L. Price, and N. Zaitlen. GBAT:  
510 a gene-based association test for robust detection of trans-gene regulation. *Genome Biol*, 21(1):211, Aug  
511 2020.
- 512 [21] H. J. Westra, M. J. Peters, T. Esko, H. Yaghoobkar, C. Schurmann, J. Kettunen, M. W. Christiansen,  
513 B. P. Fairfax, K. Schramm, J. E. Powell, A. Zhernakova, D. V. Zhernakova, J. H. Veldink, L. H. Van den  
514 Berg, J. Karjalainen, S. Withoff, A. G. Uitterlinden, A. Hofman, F. Rivadeneira, P. A. C. ' Hoen,  
515 E. Reinmaa, K. Fischer, M. Nelis, L. Milani, D. Melzer, L. Ferrucci, A. B. Singleton, D. G. Hernandez,  
516 M. A. Nalls, G. Homuth, M. Nauck, D. Radke, U. Iker, M. Perola, V. Salomaa, J. Brody, A. Suchy-Dicey,  
517 S. A. Gharib, D. A. Enquobahrie, T. Lumley, G. W. Montgomery, S. Makino, H. Prokisch, C. Herder,  
518 M. Roden, H. Grallert, T. Meitinger, K. Strauch, Y. Li, R. C. Jansen, P. M. Visscher, J. C. Knight,  
519 B. M. Psaty, S. Ripatti, A. Teumer, T. M. Frayling, A. Metspalu, J. B. J. van Meurs, and L. Franke.  
520 Systematic identification of trans eQTLs as putative drivers of known disease associations. *Nat Genet*,  
521 45(10):1238–1243, Oct 2013.
- 522 [22] Y. Gilad, S. A. Rifkin, and J. K. Pritchard. Revealing the architecture of gene regulation: the promise  
523 of eQTL studies. *Trends Genet*, 24(8):408–415, Aug 2008.
- 524 [23] Aparna Nathan, Samira Asgari, Kazuyoshi Ishigaki, Cristian Valencia, Tiffany Amariuta, Yang Luo,  
525 Jessica I Beynor, Yuriy Baglaenko, Sara Suliman, Alkes L Price, et al. Single-cell eqtl models reveal  
526 dynamic t cell state dependence of disease loci. *Nature*, 606(7912):120–128, 2022.
- 527 [24] E. Sollis, A. Mosaku, A. Abid, A. Buniello, M. Cerezo, L. Gil, T. Groza, O. §, P. Hall, J. Hayhurst,  
528 A. Ibrahim, Y. Ji, S. John, E. Lewis, J. A. L. MacArthur, A. McMahon, D. Osumi-Sutherland,  
529 K. Panoutsopoulou, Z. Pendlington, S. Ramachandran, R. Stefancsik, J. Stewart, P. Whetzel, R. Wilson,  
530 L. Hindorff, F. Cunningham, S. A. Lambert, M. Inouye, H. Parkinson, and L. W. Harris. The NHGRI-EBI  
531 GWAS Catalog: knowledgebase and deposition resource. *Nucleic Acids Res*, 51(D1):D977–D985, Jan  
532 2023.
- 533 [25] R. J. F. Loos and G. S. H. Yeo. The genetics of obesity: from discovery to biology. *Nat Rev Genet*,  
534 23(2):120–133, Feb 2022.
- 535 [26] R. K. Singh, P. Kumar, and K. Mahalingam. Molecular genetics of human obesity: A comprehensive  
536 review. *C R Biol*, 340(2):87–108, Feb 2017.
- 537 [27] P. Arner. Obesity—a genetic disease of adipose tissue? *Br J Nutr*, 83 Suppl 1:9–16, Mar 2000.
- 538 [28] Mark P Keller, Mary E Rabaglia, Kathryn L Schueler, Donnie S Stapleton, Daniel M Gatti, Matthew

- 539 Vincent, Kelly A Mitok, Ziyue Wang, Takanao Ishimura, Shane P Simonett, et al. Gene loci associated  
540 with insulin secretion in islets from nondiabetic mice. *The Journal of Clinical Investigation*, 129(10):4419–  
541 4432, 2019.
- 542 [29] G. A. Churchill, D. M. Gatti, S. C. Munger, and K. L. Svenson. The Diversity Outbred mouse population.  
543 *Mamm Genome*, 23(9-10):713–718, Oct 2012.
- 544 [30] Elissa J Chesler, Darla R Miller, Lisa R Branstetter, Leslie D Galloway, Barbara L Jackson, Vivek M  
545 Philip, Brynn H Voy, Cymbeline T Culiat, David W Threadgill, Robert W Williams, et al. The  
546 collaborative cross at oak ridge national laboratory: developing a powerful resource for systems genetics.  
547 *Mammalian Genome*, 19:382–389, 2008.
- 548 [31] Michael C Saul, Vivek M Philip, Laura G Reinholdt, and Elissa J Chesler. High-diversity mouse  
549 populations for complex traits. *Trends in Genetics*, 35(7):501–514, 2019.
- 550 [32] D. W. Threadgill, D. R. Miller, G. A. Churchill, and F. P. de Villena. The collaborative cross: a  
551 recombinant inbred mouse population for the systems genetic era. *ILAR J*, 52(1):24–31, 2011.
- 552 [33] S. M. Clee and A. D. Attie. The genetic landscape of type 2 diabetes in mice. *Endocr Rev*, 28(1):48–83,  
553 Feb 2007.
- 554 [34] K. W. Broman, D. M. Gatti, P. Simecek, N. A. Furlotte, P. Prins, Š. Sen, B. S. Yandell, and G. A.  
555 Churchill. R/qt12: Software for Mapping Quantitative Trait Loci with High-Dimensional Data and  
556 Multiparent Populations. *Genetics*, 211(2):495–502, Feb 2019.
- 557 [35] Klaasjan G Ouwens, Rick Jansen, Michel G Nivard, Jenny van Dongen, Maia J Frieser, Jouke-Jan  
558 Hottenga, Wibowo Arindrarto, Annique Claringbould, Maarten van Iterson, Hailiang Mei, et al. A  
559 characterization of cis-and trans-heritability of rna-seq-based gene expression. *European Journal of  
560 Human Genetics*, 28(2):253–263, 2020.
- 561 [36] Alkes L Price, Agnar Helgason, Gudmar Thorleifsson, Steven A McCarroll, Augustine Kong, and Kari  
562 Stefansson. Single-tissue and cross-tissue heritability of gene expression via identity-by-descent in related  
563 or unrelated individuals. *PLoS genetics*, 7(2):e1001317, 2011.
- 564 [37] Julien Bryois, Alfonso Buil, David M Evans, John P Kemp, Stephen B Montgomery, Donald F Conrad,  
565 Karen M Ho, Susan Ring, Matthew Hurles, Panos Deloukas, et al. Cis and trans effects of human  
566 genomic variants on gene expression. *PLoS genetics*, 10(7):e1004461, 2014.
- 567 [38] M. Helmer, S. Warrington, A. R. Mohammadi-Nejad, J. L. Ji, A. Howell, B. Rosand, A. Anticevic,

- 568 S. N. Sotiropoulos, and J. D. Murray. On the stability of canonical correlation analysis and partial least  
569 squares with application to brain-behavior associations. *Commun Biol*, 7(1):217, Feb 2024.
- 570 [39] Gennady Korotkevich, Vladimir Sukhov, and Alexey Sergushichev. Fast gene set enrichment analysis.  
571 *bioRxiv*, 2019.
- 572 [40] A. Subramanian, P. Tamayo, V. K. Mootha, S. Mukherjee, B. L. Ebert, M. A. Gillette, A. Paulovich,  
573 S. L. Pomeroy, T. R. Golub, E. S. Lander, and J. P. Mesirov. Gene set enrichment analysis: a  
574 knowledge-based approach for interpreting genome-wide expression profiles. *Proc Natl Acad Sci U S A*,  
575 102(43):15545–15550, Oct 2005.
- 576 [41] S. Subramanian and A. Chait. The effect of dietary cholesterol on macrophage accumulation in adipose  
577 tissue: implications for systemic inflammation and atherosclerosis. *Curr Opin Lipidol*, 20(1):39–44, Feb  
578 2009.
- 579 [42] I. Akoumianakis, N. Akawi, and C. Antoniades. Exploring the Crosstalk between Adipose Tissue and  
580 the Cardiovascular System. *Korean Circ J*, 47(5):670–685, Sep 2017.
- 581 [43] I. S. Stafeev, A. V. Vorotnikov, E. I. Ratner, M. Y. Menshikov, and Y. V. Parfyonova. Latent Inflammation  
582 and Insulin Resistance in Adipose Tissue. *Int J Endocrinol*, 2017:5076732, 2017.
- 583 [44] I. P. Fischer, M. Irmler, C. W. Meyer, S. J. Sachs, F. Neff, M. de Angelis, J. Beckers, M. H. p, S. M.  
584 Hofmann, and S. Ussar. A history of obesity leaves an inflammatory fingerprint in liver and adipose  
585 tissue. *Int J Obes (Lond)*, 42(3):507–517, Mar 2018.
- 586 [45] S. Chung, H. Cuffe, S. M. Marshall, A. L. McDaniel, J. H. Ha, K. Kavanagh, C. Hong, P. Tontonoz,  
587 R. E. Temel, and J. S. Parks. Dietary cholesterol promotes adipocyte hypertrophy and adipose tissue  
588 inflammation in visceral, but not in subcutaneous, fat in monkeys. *Arterioscler Thromb Vasc Biol*,  
589 34(9):1880–1887, Sep 2014.
- 590 [46] V. Kus, T. Prazak, P. Brauner, M. Hensler, O. Kuda, P. Flachs, P. Janovska, D. Medrikova, M. Rossmeisl,  
591 Z. Jilkova, B. Stefl, E. Pastalkova, Z. Drahota, J. Houstek, and J. Kopecky. Induction of muscle  
592 thermogenesis by high-fat diet in mice: association with obesity-resistance. *Am J Physiol Endocrinol  
593 Metab*, 295(2):E356–367, Aug 2008.
- 594 [47] C. B. Newgard. Interplay between lipids and branched-chain amino acids in development of insulin  
595 resistance. *Cell Metab*, 15(5):606–614, May 2012.
- 596 [48] D. D. Sears, G. Hsiao, A. Hsiao, J. G. Yu, C. H. Courtney, J. M. Ofrecio, J. Chapman, and S. Subramaniam.

- 597 Mechanisms of human insulin resistance and thiazolidinedione-mediated insulin sensitization. *Proc Natl*  
598 *Acad Sci U S A*, 106(44):18745–18750, Nov 2009.
- 599 [49] R. Stienstra, C. Duval, M. ller, and S. Kersten. PPARs, Obesity, and Inflammation. *PPAR Res*,  
600 2007:95974, 2007.
- 601 [50] O. Gavrilova, M. Haluzik, K. Matsusue, J. J. Cutson, L. Johnson, K. R. Dietz, C. J. Nicol, C. Vinson,  
602 F. J. Gonzalez, and M. L. Reitman. Liver peroxisome proliferator-activated receptor gamma contributes  
603 to hepatic steatosis, triglyceride clearance, and regulation of body fat mass. *J Biol Chem*, 278(36):34268–  
604 34276, Sep 2003.
- 605 [51] K. Matsusue, M. Haluzik, G. Lambert, S. H. Yim, O. Gavrilova, J. M. Ward, B. Brewer, M. L. Reitman,  
606 and F. J. Gonzalez. Liver-specific disruption of PPARgamma in leptin-deficient mice improves fatty  
607 liver but aggravates diabetic phenotypes. *J Clin Invest*, 111(5):737–747, Mar 2003.
- 608 [52] D. Patsouris, J. K. Reddy, M. ller, and S. Kersten. Peroxisome proliferator-activated receptor alpha  
609 mediates the effects of high-fat diet on hepatic gene expression. *Endocrinology*, 147(3):1508–1516, Mar  
610 2006.
- 611 [53] S. E. Schadinger, N. L. Bucher, B. M. Schreiber, and S. R. Farmer. PPARgamma2 regulates lipogenesis  
612 and lipid accumulation in steatotic hepatocytes. *Am J Physiol Endocrinol Metab*, 288(6):E1195–1205,  
613 Jun 2005.
- 614 [54] W. Motomura, M. Inoue, T. Ohtake, N. Takahashi, M. Nagamine, S. Tanno, Y. Kohgo, and T. Okumura.  
615 Up-regulation of ADRP in fatty liver in human and liver steatosis in mice fed with high fat diet. *Biochem*  
616 *Biophys Res Commun*, 340(4):1111–1118, Feb 2006.
- 617 [55] A. Srivastava, A. P. Morgan, M. L. Najarian, V. K. Sarsani, J. S. Sigmon, J. R. Shorter, A. Kashfeen,  
618 R. C. McMullan, L. H. Williams, P. guez, M. T. Ferris, P. Sullivan, P. Hock, D. R. Miller, T. A. Bell,  
619 L. McMillan, G. A. Churchill, and F. P. de Villena. Genomes of the Mouse Collaborative Cross. *Genetics*,  
620 206(2):537–556, Jun 2017.
- 621 [56] A. Roberts, F. Pardo-Manuel de Villena, W. Wang, L. McMillan, and D. W. Threadgill. The poly-  
622 morphism architecture of mouse genetic resources elucidated using genome-wide resequencing data:  
623 implications for QTL discovery and systems genetics. *Mamm Genome*, 18(6-7):473–481, Jul 2007.
- 624 [57] G. A. Churchill, D. C. Airey, H. Allayee, J. M. Angel, A. D. Attie, J. Beatty, W. D. Beavis, J. K.  
625 Belknap, B. Bennett, W. Berrettini, A. Bleich, M. Bogue, K. W. Broman, K. J. Buck, E. Buckler,  
626 M. Burmeister, E. J. Chesler, J. M. Cheverud, S. Clapcote, M. N. Cook, R. D. Cox, J. C. Crabbe,

- 627 W. E. Crusio, A. Darvasi, C. F. Deschepper, R. W. Doerge, C. R. Farber, J. Forejt, D. Gaile, S. J.  
628 Garlow, H. Geiger, H. Gershenfeld, T. Gordon, J. Gu, W. Gu, G. de Haan, N. L. Hayes, C. Heller,  
629 H. Himmelbauer, R. Hitzemann, K. Hunter, H. C. Hsu, F. A. Iraqi, B. Ivandic, H. J. Jacob, R. C. Jansen,  
630 K. J. Jepsen, D. K. Johnson, T. E. Johnson, G. Kempermann, C. Kendzierski, M. Kotb, R. F. Kooy,  
631 B. Llamas, F. Lammert, J. M. Lassalle, P. R. Lowenstein, L. Lu, A. Lusis, K. F. Manly, R. Marcucio,  
632 D. Matthews, J. F. Medrano, D. R. Miller, G. Mittelman, B. A. Mock, J. S. Mogil, X. Montagutelli,  
633 G. Morahan, D. G. Morris, R. Mott, J. H. Nadeau, H. Nagase, R. S. Nowakowski, B. F. O'Hara, A. V.  
634 Osadchuk, G. P. Page, B. Paigen, K. Paigen, A. A. Palmer, H. J. Pan, L. Peltonen-Palotie, J. Peirce,  
635 D. Pomp, M. Praveneč, D. R. Prows, Z. Qi, R. H. Reeves, J. Roder, G. D. Rosen, E. E. Schadt, L. C.  
636 Schalkwyk, Z. Seltzer, K. Shimomura, S. Shou, M. J. ä, L. D. Siracusa, H. W. Snoek, J. L. Spearow,  
637 K. Svenson, L. M. Tarantino, D. Threadgill, L. A. Toth, W. Valdar, F. P. de Villena, C. Warden,  
638 S. Whatley, R. W. Williams, T. Wiltshire, N. Yi, D. Zhang, M. Zhang, and F. Zou. The Collaborative  
639 Cross, a community resource for the genetic analysis of complex traits. *Nat Genet*, 36(11):1133–1137,  
640 Nov 2004.
- 641 [58] J. Y. Huh, Y. J. Park, M. Ham, and J. B. Kim. Crosstalk between adipocytes and immune cells in  
642 adipose tissue inflammation and metabolic dysregulation in obesity. *Mol Cells*, 37(5):365–371, May 2014.
- 643 [59] J. Lamb, E. D. Crawford, D. Peck, J. W. Modell, I. C. Blat, M. J. Wrobel, J. Lerner, J. P. Brunet,  
644 A. Subramanian, K. N. Ross, M. Reich, H. Hieronymus, G. Wei, S. A. Armstrong, S. J. Haggarty,  
645 P. A. Clemons, R. Wei, S. A. Carr, E. S. Lander, and T. R. Golub. The Connectivity Map: using  
646 gene-expression signatures to connect small molecules, genes, and disease. *Science*, 313(5795):1929–1935,  
647 Sep 2006.
- 648 [60] Aravind Subramanian, Rajiv Narayan, Steven M Corsello, David D Peck, Ted E Natoli, Xiaodong Lu,  
649 Joshua Gould, John F Davis, Andrew A Tubelli, Jacob K Asiedu, et al. A next generation connectivity  
650 map: L1000 platform and the first 1,000,000 profiles. *Cell*, 171(6):1437–1452, 2017.
- 651 [61] X. Liu, Y. I. Li, and J. K. Pritchard. Trans Effects on Gene Expression Can Drive Omnipotent Inheritance.  
652 *Cell*, 177(4):1022–1034, May 2019.
- 653 [62] U. Vosa, A. Claringbould, H. J. Westra, M. J. Bonder, P. Deelen, B. Zeng, H. Kirsten, A. Saha,  
654 R. Kreuzhuber, S. Yazar, H. Brugge, R. Oelen, D. H. de Vries, M. G. P. van der Wijst, S. Kasela,  
655 N. Pervjakova, I. Alves, M. J. é, M. Agbessi, M. W. Christiansen, R. Jansen, I. ä, L. Tong, A. Teumer,  
656 K. Schramm, G. Hemani, J. Verlouw, H. Yaghootkar, R. nmez Flitman, A. Brown, V. Kukushkina,  
657 A. Kalnayenakis, S. eger, E. Porcu, J. Kronberg, J. Kettunen, B. Lee, F. Zhang, T. Qi, J. A. Hernandez,

- 658 W. Arindrarto, F. Beutner, J. Dmitrieva, M. Elansary, B. P. Fairfax, M. Georges, B. T. Heijmans, A. W.  
659 Hewitt, M. nen, Y. Kim, J. C. Knight, P. Kovacs, K. Krohn, S. Li, M. Loeffler, U. M. Marigorta, H. Mei,  
660 Y. Momozawa, M. ller Nurasyid, M. Nauck, M. G. Nivard, B. W. J. H. Penninx, J. K. Pritchard, O. T.  
661 Raitakari, O. Rotzschke, E. P. Slagboom, C. D. A. Stehouwer, M. Stumvoll, P. Sullivan, P. A. C. 't Hoen,  
662 J. Thiery, A. njes, J. van Dongen, M. van Iterson, J. H. Veldink, U. lker, R. Warmerdam, C. Wijmenga,  
663 M. Swertz, A. Andiappan, G. W. Montgomery, S. Ripatti, M. Perola, Z. Katalik, E. Dermitzakis,  
664 S. Bergmann, T. Frayling, J. van Meurs, H. Prokisch, H. Ahsan, B. L. Pierce, T. ki, D. I. Boomsma, B. M.  
665 Psaty, S. A. Gharib, P. Awadalla, L. Milani, W. H. Ouwehand, K. Downes, O. Stegle, A. Battle, P. M.  
666 Visscher, J. Yang, M. Scholz, J. Powell, G. Gibson, T. Esko, L. Franke, P. A. C. 't Hoen, J. van Meurs,  
667 J. van Dongen, M. van Iterson, M. A. Swertz, and M. Jan Bonder. Large-scale cis- and trans-eQTL  
668 analyses identify thousands of genetic loci and polygenic scores that regulate blood gene expression. *Nat*  
669 *Genet*, 53(9):1300–1310, Sep 2021.
- 670 [63] B. Hallgrímsson, R. M. Green, D. C. Katz, J. L. Fish, F. P. Bernier, C. C. Roseman, N. M. Young,  
671 J. M. Cheverud, and R. S. Marcucio. The developmental-genetics of canalization. *Semin Cell Dev Biol*,  
672 88:67–79, Apr 2019.
- 673 [64] M. L. Siegal and A. Bergman. Waddington's canalization revisited: developmental stability and evolution.  
674 *Proc Natl Acad Sci U S A*, 99(16):10528–10532, Aug 2002.
- 675 [65] A. B. Paaby and G. Gibson. Cryptic Genetic Variation in Evolutionary Developmental Genetics. *Biology*  
676 (*Basel*), 5(2), Jun 2016.
- 677 [66] E. A. Boyle, Y. I. Li, and J. K. Pritchard. An Expanded View of Complex Traits: From Polygenic to  
678 Omnipigenic. *Cell*, 169(7):1177–1186, Jun 2017.
- 679 [67] Naomi R Wray, Cisca Wijmenga, Patrick F Sullivan, Jian Yang, and Peter M Visscher. Common disease  
680 is more complex than implied by the core gene omnipigenic model. *Cell*, 173(7):1573–1580, 2018.
- 681 [68] H. Shimizu and A. Osaki. Nesfatin/Nucleobindin-2 (NUCB2) and Glucose Homeostasis. *Curr Hypertens*  
682 *Rev*, pages Nesfatin/Nucleobindin-2 (NUCB2) and Glucose Homeostasis., Jul 2014.
- 683 [69] M. Nakata and T. Yada. Role of NUCB2/nesfatin-1 in glucose control: diverse functions in islets,  
684 adipocytes and brain. *Curr Pharm Des*, 19(39):6960–6965, 2013.
- 685 [70] M. Riva, M. D. Nitert, U. Voss, R. Sathanoori, A. Lindqvist, C. Ling, and N. Wierup. Nesfatin-1  
686 stimulates glucagon and insulin secretion and beta cell NUCB2 is reduced in human type 2 diabetic  
687 subjects. *Cell Tissue Res*, 346(3):393–405, Dec 2011.